1 Microrheology

M.L. Gardel, M.T. Valentine and D.A. Weitz

Department of Physics and Division of Engineering and Applied Sciences,
Harvard University, Cambridge MA 02138

1.1 Introduction

Rheology is the study of the deformation and flow of a material in response to applied stress. Simple solids store energy and provide a spring-like, elastic response, whereas simple liquids dissipate energy through viscous flow. For more complex viscoelastic materials, rheological measurements reveal both the solid- and fluid-like responses and generally depend on the time scale at which the sample is probed (Larson 1999). One way to characterize rheological response is to measure the shear modulus as a function of frequency. Traditionally, these measurements have been performed on several milliliters of material in a mechanical rheometer by applying a small amplitude oscillatory shear strain, $\gamma(t) = \gamma_o \sin(\omega t)$ where γ_o is the amplitude and ω is the frequency of oscillation, and measuring the resultant shear stress. Typically, commercial rheometers probe frequencies up to tens of Hz. The upper range is limited by the onset of inertial effects, when the oscillatory shear wave decays appreciably before propagating throughout the entire sample. If the shear strain amplitude is small, the structure is not significantly deformed and the material remains in equilibrium; in this case, the affine deformation of the material controls the measured stress. The time-dependent stress is linearly proportional to the strain, and is given by:

$$\sigma(t) = \gamma_o \left[G'(\omega)\sin(\omega t) + G''(\omega)\cos(\omega t) \right] \tag{1.1}$$

$G'(\omega)$ is the response in phase with the applied strain and is called the elastic or storage modulus, a measure of the storage of elastic energy by the sample. $G''(\omega)$ is the response out of phase with the applied strain, and in phase with the strain rate, and is called the viscous or loss modulus, a measure of viscous dissipation of energy. The complex shear modulus is defined as $G^* \equiv G' + iG''$. Alternatively, it is possible to apply stress and measure strain and obtain equivalent material properties.

Rheology measurements such as these have given valuable insight into the structural rearrangements and mechanical response of a wide range of materials. They are particularly valuable in characterizing soft materials or complex fluids, such as colloidal suspensions, polymer solutions and gels, emulsions, and surfactant mixtures (Ferry 1980, Macosko 1994, Larson 1999). However, conventional mechanical techniques are not always well-suited for all systems. Typically, milliliter sample volumes are required, precluding the study of rare or precious materials, including many biological samples that are difficult to obtain in large quantities. Moreover, conventional rheometers provide an average measurement of the bulk response, and do not allow for local measurements in inhomogeneous systems. To address these issues, a new class of microrheology measurement techniques has emerged. To probe the material response on micrometer length scales with microliter sample volumes. Microrheology methods typically use embedded micron-sized probes to locally deform a sample. There are two broad classes of micro-rheology techniques: those involving the active manipulation of probes by the local application of stress and those measuring the passive motions of particles due to thermal or Brownian fluctuations. In either case, when the embedded particles are much larger than any structural size of the material, particle motions measure the macroscopic stress relaxation; smaller particles measure the local mechanical response and also probe the effect of steric hindrances caused by local microstructure. The use of small colloidal particles theoretically extends the accessible frequency range by shifting the onset of inertial effects to the MHz regime; in practice, the measurable frequency range varies with the details of the experimental apparatus.

In this chapter, we will detail a variety of microrheology methods. In Section 1.2, we review the active manipulation techniques in which stress is locally applied to the material by use of electric or magnetic fields, or micromechanical forces. These active methods often require sophisticated instrumentation and have the advantage of applying large stresses to probe stiff materials and non-equilibrium response. Often single particle measurements are possible, allowing measurements of local material properties in inhomogeneous systems. In Section 1.3, we discuss the passive measurements of thermally excited probes, in which no external force is applied. For these methods, the mean squared displacement of the probe particle is measured using various experimental techniques and related to the macroscopic linear viscoelastic moduli of the material using a generalized Stokes-Einstein relationship. In Section 1.4, we discuss the practical application of microrheology techniques to number of systems, including heterogeneous materials. In heterogeneous systems, video-based multiple particle tracking methods are used to simultaneously measure the thermally-induced motions of dozens of particles in a single field of view. Single particle data is then used to map out the spatial variations in material mechanics and microstructure. In Section 1.5, we discuss two-particle microrheology, in which the correlated motions between pairs of particles are used to measure the coarse-grained macroscopic material properties. This allows the characterization of

bulk material properties even in systems that are inhomogeneous on the length scale of the probe particle. We close the chapter with a brief summary and outlook. The experimental considerations of light scattering and particle tracking techniques are discussed in detail in the Appendix.

1.2 Active Microrheology Methods

One class of microrheology techniques involves the active manipulation of small probe particles by external forces, using magnetic fields, electric fields, or micromechanical forces. These measurements are analogous to conventional mechanical rheology techniques in which an external stress is applied to a sample, and the resultant strain is measured to obtain the shear moduli; however, in this case, micron-sized probes locally deform the material and probe the local viscoelastic response. Active measurements allow the possibility of applying large stresses to stiff materials in order obtain detectable strains. They can also be used to measure non-equilibrium behavior, as sufficiently large forces can be applied to strain the material beyond the linear regime.

1.2.1. Magnetic Manipulation Techniques

The oldest implementation of microrheology techniques involves the manipulation of magnetic particles or iron filings, which are embedded in a material, by an external magnetic field. This method was pioneered in the early 1920's and has been used to measure the mechanical properties of gelatin, cellular cytoplasm and mucus (Freundlich and Seifriz 1922, Heilbronn 1922, Crick and Hughes 1950, Yagi 1961, Hiramoto 1969, King and Macklem 1977). The visual observation of the particles' movements provided a qualitative measure of the viscoelastic response, but the irregularly shaped magnetic particles and simple detection schemes did not allow a precise measure of material properties. More recently, advances in colloidal engineering, video microscopy, and position sensitive detection have prompted the emergence of several high precision magnetic particle micro-rheological techniques.

One method called "magnetic bead microrheometry" or "magnetic tweezers" combines the use of strong magnets to manipulate embedded superparamagnetic particles, with video microscopy to measure the displacement of the particles upon application of constant or time-dependent forces (Ziemann, et al. 1994, Amblard, et al. 1996, Schmidt, et al. 1996). In this case, strong magnetic fields are required to induce a magnetic dipole in the super-paramagnetic beads, and magnetic field gradients are applied to produce a force. The resultant particle displacements measure the rheological response of the surrounding material. Magnetic tweezers techniques have been used to measure the micro-

scopic dynamics of a number of interesting materials that are not easily probed with traditional bulk techniques, including networks of filamentous actin (Ziemann, et al. 1994, Amblard, et al. 1996, Schmidt, et al. 1996, Keller, et al. 2001), living fibroblast (Bausch, et al. 1998), macrophage (Bausch, et al. 1999), endothelial (Bausch, et al. 2001) and dictyostelium cells (Feneberg, et al. 2001), and solutions of the semi-flexible filamentous bacteriophage fd (Schmidt, et al. 2000). In one experimental design, as shown in Fig. 1.1, the magnetic field is created by four pairs of soft ferromagnetic pole pieces arranged at right angles, where each pair is wound with a separate field coil (Amblard, et al. 1996). Four attached Hall probes are used to measure the local magnetic field. Each pair of poles is precisely positioned in plane and the geometric center of the pair is at the optical focus of the microscope, ensuring a negligible vertical component to the magnetic field. This design creates a uniform magnetic field parallel to the focal plane and directed to one of the poles, and allows both translation and rotation of magnetic colloidal particles, which are typically 0.5 - 5 μm in diameter. In rotation mode, the field is uniform, with controlled angle relative to the orientation of the pole pieces, making it a potentially useful tool for measuring the local bending modulus of a material. In translation mode, a large magnetic field is generated at one attracting pole; field lines that originate from the attracting pole

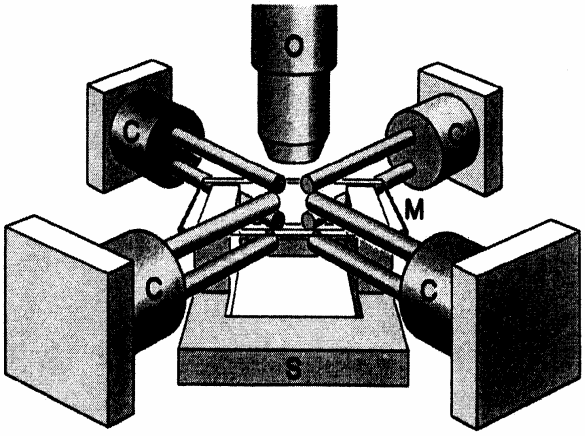

Fig. 1.1. A schematic of one experimental design of a magnetic bead microrheometer. The sample (M) is placed is the center of four coils (C) and magnetic pole pieces and supported by a sample holder (S) on an upright research microscope. The magnetic particles in the specimen plane are imaged using the objective lens (O) and particle displacements are measured with video-based detection. (Reprinted with permission from Amblard, et al 1996).

spread out to three opposing poles where smaller fields are generated. In order to generate forces, gradient fields are required, and are created by a precise balance of attracting flux and the total flux at the opposing poles. The force, $f(t)$, on the particle is given by:

$$f_x(t) = \vec{M}(t) \cdot \frac{\partial \vec{B}(t)}{\partial x} = \chi V \vec{B}(t) \cdot \frac{\partial \vec{B}(t)}{\partial x} \tag{1.2}$$

where $M(t)$ is the induced magnetic moment of the particle, $B(t)$ is the is the imposed magnetic field, χ is the susceptibility of the particle and V is the volume of the particle. Typically, for 0.1-0.2 T magnetic fields and 10-20 T/m gradients, applied forces are in the range of pN and torques are in the range of 10^{-14} N·m.

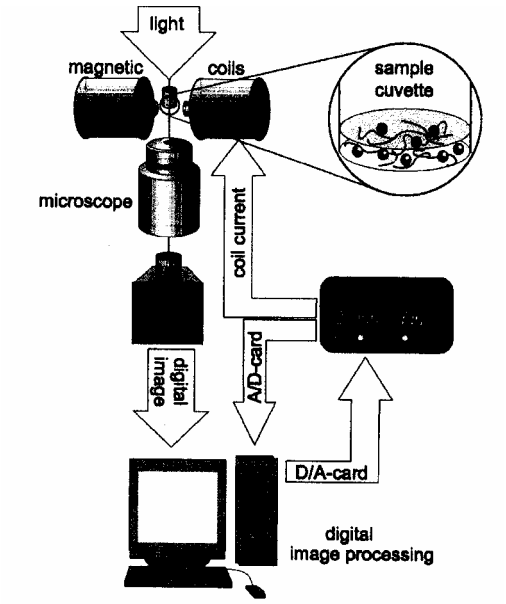

Fig. 1.2. A schematic view of one of the experimental designs of a magnetic bead microrheometer. The magnet consists of two coils with cylindrical soft iron cores. The sample and magnet are mounted on an inverted research microscope. A CCD camera is used to capture images of the particle and image analysis routines are used to measure particle displacements. The amplifier used to drive the magnet's power supply also delivers a signal to the computer to allow measurements of phase lag. (reprinted with permission from Keller, et al 2001).

A second design, shown in Fig. 1.2, uses one or two axisymmetrically arranged magnetic coils with soft iron cores that apply a field gradient to produce a force in the focal plane (Ziemann, et al. 1994, Schmidt, et al. 1996, Keller, et al. 2001). The force exerted depends on the details of the tip geometry, but is typically in the range of 10 pN to 10 nN. For higher forces, only one coil is used and the tip of the pole piece is positioned as close as 10 μm to the magnetic particle. Typically, the magnetic particles are separated by more than 50 μm and only single particle displacements are recorded to prevent neighboring spheres from creating induced dipolar fields. In both designs, video microscopy is used to detect the displacements of the particles under application of force. The instrumental precision depends on the details of the design and will be discussed in detail in Sec A.3; however, the spatial resolution is typically in the range of 10-20 nm and the temporal dynamic range is 0.01-100 Hz. Three modes of operation are available in any rheology measurement performed under applied force: a viscometry measurement obtained by applying constant force, a creep response measurement after the application of a pulse-like excitation, or a measurement of the frequency dependent viscoelastic moduli in response to an oscillatory stress. In constant force mode, the viscosity of a Newtonian fluid is measured by balancing the external driving force with the viscous drag force experienced by the particle as it moves through the fluid; because the particles are

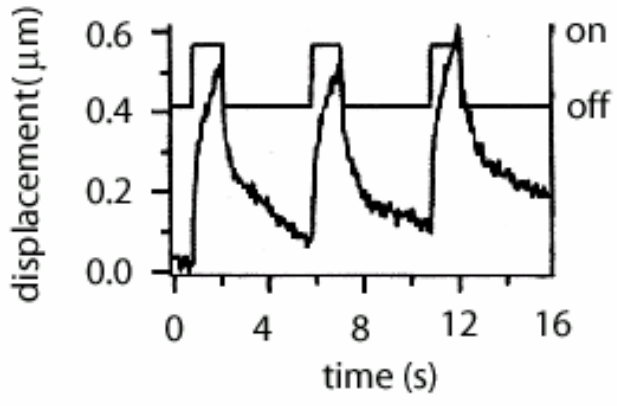

Fig. 1.3. A typical creep response and recovery curve from a magnetic particle measurement. The step pulses indicate the application of stress by turning on and off the external magnetic field. The resultant bead displacement consists of a fast elastic response at the initial onset of stress, followed by a slowing down and viscous flow regime. (reprinted with permission from Bausch, et. al. 1999)

so small and light, inertial effects are typically ignored. The equation of motion is given by Stoke's Law, $f_o = 6\pi\eta a v$, where f_o is the constant external force, η is the fluid viscosity, a is the particle radius and v is the velocity with which the particle moves through the fluid. By using a fluid of known viscosity, this measurement also allows for the calibration of the force exerted on the particle by a given coil current.

In addition to constant force viscometry measurements, time-dependent forces can be applied to measure the frequency dependent viscoelastic response. In a creep-response measurement, a force pulse is applied to the particle and the particle deflection is measured as a function of time. Representative data curves are shown in Fig. 1.3. The time dependence of the bead deflection, $x_d(t)$ can be expressed as:

$$x_d(t) = J(t)\frac{f(t)}{6\pi a} \tag{1.3}$$

where $J(t)$ is the time-dependent creep compliance of the material in which the bead is embedded. In many cases, $J(t)$ can be interpreted with the use of mechanical equivalent circuits of springs, which represent elastic storage, and dashpots, which represent viscous loss, to model the local mechanical response (Ferry 1980, Bausch, et al. 1998). Alternatively, an oscillatory force can be applied to drive the particle at a controlled amplitude and frequency. The amplitude and phase shift of the particle's displacement with respect to the driving force are measured and are used to calculate the local frequency-dependent viscoelastic moduli. When an oscillatory force, $f(t) = f_0 \exp(i\omega t)$ is applied to the particles, the displacement can be expressed as $x(t) = x_0 \exp\left[i(\omega t - \varphi)\right]$ and the shear moduli are given by:

$$G'(\omega) = \frac{f_o}{6\pi a\left|x_o\omega\right|}\cdot\cos\varphi(\omega)$$
$$G''(\omega) = \frac{f_o}{6\pi a\left|x_o\omega\right|}\cdot\sin\varphi(\omega) \tag{1.4}$$

If the probe particles are larger than all length scales of the material, then the measured shear moduli report the macroscopic bulk response. If however, the particles are embedded in an inhomogeneous material, then each particle measures the dynamic microenvironment that surrounds it and the local material response. In materials that actively change in response to external stimuli, real-time measurements of the local dynamics are possible (Bausch, et al. 2001).

Local properties can be further probed by measuring the strain field around the each particle using mixtures of paramagnetic particles and non-magnetic latex spheres (Schmidt, et al. 1996, Bausch, et al. 1998). The magnetic particles are displaced by application of constant force and the resultant deformation field is visualized by measuring the movements of the surrounding latex particles. For a homogeneous elastic material, the deformation field is given by:

$$\vec{u} = \frac{1+\sigma}{8\pi E(1-\sigma)} \frac{(3-4\sigma)\vec{f} + \hat{r}(\hat{r}\cdot\vec{f})}{r} \tag{1.5}$$

where r is the distance from the point source, $\hat{r}$ is a unit vector in the direction of r, σ is the Poisson ratio, E is the Young's modulus (Landau and Lifshitz 1986). The elastic constants E and σ are measured, and from these the time-independent shear modulus is derived: $\mu = E/2(1+\sigma)$. Any deviations from the $1/r$ spatial decay in the strain field indicate the presence of local heterogeneities.

In addition to magnetic tweezers methods, a number of other magnetic particle techniques have been developed to measure material response. Twisting magnetometry measures the response of magnetic inclusions in a viscous or viscoelastic body to the brief application of a strong external magnetic field (Valberg 1984, Valberg and Albertini 1985, Valberg and Butler 1987, Valberg and Feldman 1987, Zaner and Valberg 1989). The strong field aligns the magnetic moments of the inclusions, which can be magnetic colloidal particles or polycrystalline iron oxide particles or aggregates. After the field is turned off, the aligned magnetic moments give rise to measurable magnetic field, the "remnant" field, which decays as the moments become randomized. In cases where rotational diffusion is the dominant randomizing agent, the decay can be interpreted in terms of the local viscosity. Viscoelastic response can also be measured by incorporating a weaker twisting field, in a direction perpendicular to the initial strong magnetic field (Zaner and Valberg 1989). When the twisting field is first applied, it lies in a direction perpendicular to the magnetic moments of the particles and the torque on the particles is maximal, causing the particles to rotate toward the direction of the weaker twisting field. The rate at which the particles align with the twisting field and the amount of recoil after the twisting field is turned off give a measure of local viscosity and elasticity. An in-line magnetometer allows the measurement of the angular strain and thus the local compliance, defined as a ratio of applied stress to strain.

A modification of the twisting magnetometry technique, called magnetic twisting cytometry, has been used to apply mechanical stresses directly to cell surface receptors using ligand coated magnetic colloidal particles that are deposited on the surface of a living cell (Wang, et al. 1993, Wang and Ingber 1994, Wang and Ingber 1995). The ferromagnetic particles are magnetized in one direction, and then twisted in a perpendicular direction to apply a controlled shear

stress to the cell surface; as the particles re-orient, a magnetometer measures the change in remnant field, which is related to the angular strain. Alternatively, the twisting cytometry measurements can be mounted on a research microscope, and the particle displacements measured with video microscopy (Fabry, et al. 2001). When the twisting magnetic field is made to vary sinusoidally in time, bead displacement can be interpreted in terms of the local viscoelastic response (Fabry, et al. 2001). The frequency dependence of the material response can be obtained directly; however, in order to calculate the stress exerted on the cell surface by the particle and the absolute viscoelastic moduli, the details of the contact area and amount of particle embedding in the cell surface must be known.

Magnetic particle techniques allow measurements of bulk rheological response in homogeneous materials or local response in heterogeneous samples. Strain-field mapping identifies heterogeneities and allows the measurement of local microstructure and real-time measurements characterize dynamic changes in material response. Because such small sample volumes are required and non-invasive magnetic fields are used, these techniques are particularly useful for studying biological materials.

1.2.2 Optical Tweezers Measurements

Another active manipulation technique uses optical tweezers, also called optical traps or laser tweezers, that employ highly focused beams of light to capture and manipulate small dielectric particles (Ashkin 1992, Block 1992, Ashkin 1997, Ashkin 1998). Unlike magnetic tweezers, optical tweezers apply force very locally and the forces are typically limited to the pN range. The two main optical forces exerted on the illuminated particle are the scattering force, or radiation pressure, which acts along the direction of beam propagation, and the gradient force, which arises from induced dipole interactions with the electric field gradient and tends to pull particles toward the focus (Ashkin 1992, Ashkin 1997, Nemoto and Togo 1998, Neto and Nussenzveig 2000). Steep electric field gradients can be created using a high numerical aperture objective lens to focus a laser beam onto the sample; this allows the gradient force to dominate and forms a stable three-dimensional trap. Moving the focused laser beam forces the particle to move, apply local stress to the surrounding material, and probe the local rheological response.

The experimental design is typically based on an inverted optical microscope with a quality high numerical aperture oil-immersion objective lens (Fällman and Axner 1997, Visscher and Block 1998, Mio, et al. 2000, Mio and Marr 2000). The microscope allows for simultaneous imaging of the sample and facilitates placement of the beam in an inhomogeneous material. The illuminating laser beam is steered into the microscope with an external optical train, and is commonly introduced from the epi-fluorescence port and deflected into the opti-

cal path of the microscope by a dichroic mirror located below the objective lens. In order to achieve the most efficient and stable trapping, the beam is collimated at the back focal plane (BFP) of the objective and the objective entrance aperture is slightly overfilled. The external optical train allows the control of beam placement and movement, and even remote control of beam movement through the use of piezo-controlled mirror mounts or acousto-optic modulators. Steering mirrors are placed in a plane conjugate to the BFP of the objective to ensure that the intensity and strength of the laser trap does not fluctuate as the beam is moved (Fällman and Axner 1997). The slight tilting of a mirror in this plane will result in a corresponding change only in the direction of the laser beam at the BFP of the objective, maintaining a constant degree of overfilling at the entrance aperture and resulting only in the lateral movement of the optical trap in the specimen plane.

At the center of the optical trap, which is typically located slightly above the focal plane, the gradient and scattering forces balance and the net optical force is zero. At the trap center, the potential energy is given by:

$$U = \frac{-3V_p n_1}{c}\left(\frac{n_2^2 - n_1^2}{n_2^2 + 2n_1^2}\right) I_o e^{-r^2/R^2} \tag{1.6}$$

where V_p is the volume of the particle, n_2 is the index of refraction of the particle and n_1 is the index of refraction of the surrounding fluid, r is the radial distance from the center of the trap and R is the $1/e$ width of the Gaussian laser profile at the trap (Ou-Yang 1999). For stable trapping, $n_1 > n_2$ is required. The force on the particle as it moves from the trap center is given by:

$$\begin{aligned} F &= -\nabla U \\ &= -\frac{6rV_p n_1}{cR^2} I_o \left(\frac{n_2^2 - n_1^2}{n_2^2 + 2n_1^2}\right) e^{-r^2/R^2} \hat{r} \\ &\equiv k_{ot} r e^{-r^2/R^2} \hat{r} \end{aligned} \tag{1.7}$$

and for small displacements, the force is approximated by Hooke's law with an effective spring constant, k_{ot} (Ou-Yang 1999). Thus, if the laser beam center is offset from the center of the particle, the particle experiences a restoring force toward the center of the trap. By moving the trap with respect to the position of the bead, stress can be applied locally to the sample, and the resultant particle displacement reports the strain, from which rheological information can be obtained.

In order to apply a known force, the trap spring constant, k_{ot}, must be measured. There are several methods for calibration of k_{ot}, which is typically linearly dependent on the intensity of the incident laser beam. The escape force method

measures the amount of force needed to remove a sphere from the trap. Although this method is simple and doesn't require a sophisticated detection scheme for measuring small displacements, it depends critically on the shape of the potential at large displacements where the trapping force response is likely non-linear. If high resolution position detection methods are available, the trap spring constant may be measured by slowly flowing a fluid of known viscosity past the trapped particle and measuring the displacement of the particle due to the viscous drag force. For small displacements, the viscous drag force can be balanced by the linear restoring force of the trap, and the trap spring constant can be determined. Alternatively, k_{ot} can be measured from the thermal fluctuations in the position of the trapped particle. The trap spring constant is calculated using the equipartition theorem:

$$\tfrac{1}{2} k_B T = \tfrac{1}{2} k_{ot} \left\langle x^2 \right\rangle \tag{1.8}$$

where x is the particle position and $k_B T$ is the thermal energy.

For measurements of rheological properties, particle displacements in response to an applied force must be precisely detected. Position detection methods fall into two broad categories: direct imaging methods and laser-based detection schemes. Direct imaging can be achieved using video microscopy to record images of trapped particles in the specimen plane and centroid tracking algorithms to find the particle positions in each frame, typically with a spatial resolution of one-tenth of a pixel (Crocker and Grier 1996). The temporal resolution is limited by the capture rate of the camera, and is typically 30 frames per second. Alternatively, the shadow cast by the particle can be imaged onto a quadrant photodiode detector, which is aligned such that when the particle is in the center of the trap, the intensity of light on each of the four quadrants is equal (Ou-Yang 1999). As the particle moves from the trap center, the difference in light intensity on the four quadrants is recorded to measure the particle displacement. Although the direct imaging techniques are simple to implement and interpret, they do not provide the high spatial or temporal resolution of laser based detection schemes.

Interferometry detection is one laser-based detection scheme (Gittes, et al. 1997, Schnurr, et al. 1997, Visscher and Block 1998). In this design, a Wollaston prism, which is located behind the objective lens and used conventionally for Differential Interference Microscopy (DIC), splits the laser light into two orthogonally polarized beams. This produces two nearly overlapping, diffraction-limited spots in the specimen plane that act as a single optical tweezers. After passing through the sample, the beams are recombined behind the condenser lens by a second Wollaston prism; the recombined beam passes through a quarter wave plate. If the particle is centered or the optical trap is empty, then the recombined beam has the same linear polarization as the incoming beam and the final beam is circularly polarized; however, if the particle is slightly off-center

there is a phase lag introduced between the two beams and final beam is elliptically polarized. The degree of ellipticity gives a measure of the particle displacement. The response is linear for displacements of up to 200 nm for 500 nm particles and larger particles have an extended linear range; larger displacements may be detected using a piezo-activated stage to realign the particle with the center of the laser beam. Data is typically acquired at rates of 50-60 kHz, with subnanometer resolution (Gittes, et al. 1997, Schnurr, et al. 1997). This interferometry design has the advantages of high sensitivity and inherent alignment; however, it gives only one-dimensional data along the shear axis of the Wollaston prism.

Alternatively, the forward deflected laser light can be projected onto a photodiode to detect the displacement of the trapped particle. A trapped bead acts as a mini-lens and deflects the illuminating laser light forward through the condenser lens, which relays the light onto the photodiode. In a single photodiode configuration, the detector is positioned so that roughly 50% of the optical power from the diverging cone of light is intercepted (Visscher and Block 1998). This configuration is qualitatively sensitive to both axial displacements, which change the diameter of the intercepted light cone and the intensity of light at the detector, and lateral displacements, which offset the cross-sectional area of the light cone from the active detector area. However, quantitative measurements of particle displacements are not straightforward with single photodiode detection since axial and lateral displacements are not easily decoupled and since no information about small movements in the focal plane is available. Alternatively, quantitative sub-nanometer displacements can be measured with a quadrant photodiode placed in the BFP of the condenser lens. Typically, the active area of the detector is larger than the area of the intercepted light cone, so axial displacements are not detected. The forward-scattered light is detected by the photodiode, where the photocurrent differences are amplified and converted into voltages to measure the relative displacement of the bead with respect to the trap center. The trajectory is obtained by sampling the voltages with an A/D converter at rates up to 50 kHz. The spatiotemporal resolution is 0.01 $nm/Hz^{1/2}$ above 500 Hz; at lower frequencies, the resolution decreases and degrades to 1 $nm/Hz^{1/2}$ at 20 Hz due to the mechanical resonance of the stage (Mason, et al. 2000). The maximal displacement that may be detected with this technique is approximately 200 nm.

To measure rheological properties, optical tweezers are used to apply a stress locally by moving the laser beam and dragging the trapped particle through the surrounding material; the resultant bead displacement is interpreted in terms of viscoelastic response. Elasticity measurements are possible by applying a constant force with the optical tweezers and measuring the resultant displacement of the particle. This approach has been used to measure the time-independent shear modulus of red blood cell membranes (Hénon, et al. 1999, Sleep, et al. 1999). Alternatively, local frequency-dependent rheological properties can be measured by oscillating the laser position with an external steerable mirror and

measuring the amplitude of the bead motion and the phase shift with respect to the driving force (Valentine, et al. 1996, Ou-Yang 1999). The equation of motion for a colloidal particle in forced oscillation in a viscoelastic medium is given by:

$$m^*\ddot{x} + 6\pi\eta^* a\dot{x} + (k_{ot} + k)x = k_{ot} A\cos(\omega t) \tag{1.9}$$

where m^* is the effective mass, η^* is the effective frequency dependent viscosity of the medium, a is the particle radius, k_{ot} is the spring constant of the trap, k is the frequency dependent spring constant of the medium, A is the amplitude of the trap displacement and ω is the driving frequency (Ou-Yang 1999). The effective mass includes the bare mass of the particle and contribution of the inertia of the surrounding fluid entrained by the moving particle. The effective mass is given by:

$$m^* = m_o + \frac{2\pi}{3}a^3\rho + 3\pi a^2\sqrt{\frac{2\eta\rho}{\omega}} \tag{1.10}$$

where ρ is the mass density and η is the viscosity of the surrounding fluid. The effective viscosity also includes an inertial correction, and is given by:

$$\eta^* = \eta\left(1 + \sqrt{\frac{a^2\rho\omega}{2\eta}}\right). \tag{1.11}$$

The equation of motion can be solved by:

$$x(t) = D(\omega)\cos(\omega t - \delta(\omega)). \tag{1.12}$$

By detecting the forward-scattered light from a second weaker probing beam and using a lock-in amplifier, the relative displacement and phase are measured. With this dual beam approach, $D(\omega)$, the amplitude of the particle displacement given by:

$$D(\omega) = \frac{k_{ot} A}{\sqrt{(k_{ot} + k - m^*\omega^2)^2 + m^{*2}\beta^2\omega^2}} \tag{1.13}$$

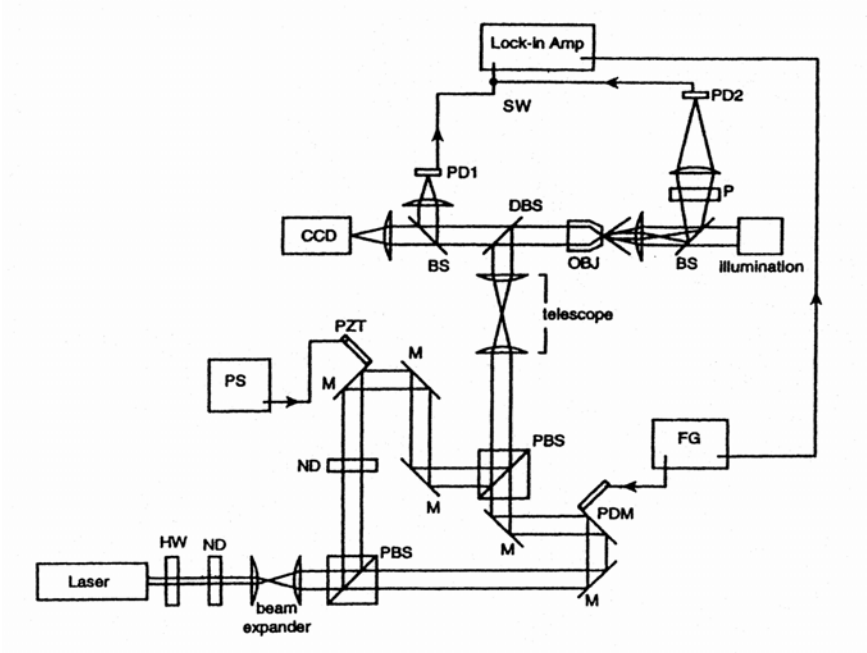

Fig. 1.4. A schematic of the experimental setup of the oscillating optical tweezers. The first polarizing beam splitter (PBS) splits the laser light into two separate beams, one stronger trapping beam and a second weaker probing beam. Both are independently aligned and steered by two piezoelectrically driven mirrors (PDM); rotation of the half-wave plate (HW) changes the relative intensity of the two beams. A function generator (FG) drives the PDM that moves the trapping beam and also delivers a signal to the lock-in amplifier, allowing the phase lag to be measured. PD1 and PD2 are quadrant photodiode detectors, and SW a switch to allow the signal from either PD1 or PD2 to reach the lock in amplifier. PD1 is used for direct imaging of the trapped particle while PD2 is used to measure the forward scattered laser light. The polarizer (P) placed before PD2 is used to select either the trapping or probing beam for position detection. ND is a neutral density filter, M a mirror, PS a power supply for the piezoelectric-driver (PZT), BS a beamsplitter, DBS a dichroic beam splitter which reflects the laser light and allows the broadband illumination light to pass. The sample chamber and trapped particle are located to the right of the high-numerical-aperture objective lens (OBJ) and are not shown. (reprinted with permission from Ou-Yang 1999).

The phase shift, $\delta(\omega)$, is given by:

$$\delta(\omega) = \tan^{-1} \frac{m^* \beta \omega}{k_{ot} + k - m^* \omega^2} \tag{1.14}$$

where $\beta = 6\pi\eta^* a / m^*$ and k_{ot} is now given by the sum of the spring constants of the two laser beams. The second probing beam is not required; the trapping beam can also be used to measure particle displacements with modified expressions for $D(\omega)$ and $\delta(\omega)$. The equations for displacement and phase are solved for the material viscosity, $\eta(\omega)$, and elasticity, $k(\omega)$, from which the frequency dependent viscoelastic moduli are derived:

$$G'(\omega) = \frac{k(\omega)}{2\pi a} \tag{1.15}$$

$$G''(\omega) = \omega(\eta(\omega) - \eta_{solvent}) \tag{1.16}$$

(Hough and Ou-Yang 1999). The typical experimental design for frequency dependent measurements is shown in Fig. 1.4. Oscillating tweezers methods have been used to study telechelic HEUR polymers (Hough and Ou-Yang 1999) and collagen gels (Velegol and Lanni 2001).

Optical tweezers techniques use single particles and provide for local measurements in inhomogeneous materials. Higher frequency measurements are possible with laser detection tweezers techniques than with video-based magnetic particle manipulation methods, and strain field mapping measurements are also possible. However, there are disadvantages: forces are limited to the pico-Newton range, local heating can occur, as well as local phototoxic effects in biological samples.

1.2.3 Atomic Force Microscopy Techniques

The third active manipulation technique employs the use of micromechanical forces created by an atomic force microscope to probe local mechanical response. The atomic force microscope (AFM), invented in 1986 (Binning, et al. 1986), has been widely used to study the structure of soft materials, and biological materials in particular, with sub-nanometer resolution (Drake, et al. 1989, Henderson, et al. 1992, Radmacher, et al. 1992, Bottomley, et al. 1996, Kasas, et al. 1997). In addition to imaging information about surface structure and topology, AFM techniques are sensitive to the force required to indent a surface and have been used to measure local elasticity and viscoelasticity of thin samples, including bone and bone marrow (Tao, et al. 1992), gelatin (Radmacher, et al.

1995, Domke and Radmacher 1998), polyacrylamide gels (Mahaffy, et al. 2000), platelets (Radmacher, et al. 1996), and living cells (Hoh and Schoenenberger 1994, Putman, et al. 1994, Shroff, et al. 1995, Goldman and Ezzell 1996, Rotsch, et al. 1997, A-Hassan, et al. 1998, Mahaffy, et al. 2000). Topographic images are obtained simultaneously with mechanical response, allowing elasticity to be correlated with local structure (Radmacher, et al. 1994). Local elasticity measurements have also provided information about the mechanical changes that accompany dynamic processes including cell division (Dvorak and Nagao 1998), activation of platelets (Radmacher, et al. 1996), exocytosis (Schneider, et al. 1997), and drug-induced changes in the cytoskeletal structure of living cells (Rotsch and Radmacher 2000).

Experimentally, a commercial AFM with soft cantilever is used in constant-force tapping mode for both imaging and elasticity measurements. The deflection of the cantilever is often measured with an optical "beam bounce" detection technique in which a laser beam bounces off the back of the cantilever onto a position sensitive photodetector. In constant force mode, the cantilever deflection is kept constant by a feedback circuit that changes the height of the piezoelectrically controlled scanner head in response to the local topography. In this mode, an image is generated from the scanner motion, and the scan speed is limited by the response time of the feedback circuit. In tapping mode, the tip of the cantilever is vibrated close to the sample surface, allowing the bottom of the tip to gently touch or "tap" the surface; the oscillation amplitude changes with tip-to-sample distance.

For each elasticity measurement, the deflection of the cantilever is measured as it approaches the sample. For small deflections, the loading force can be calculated using Hooke's law once the cantilever spring constant, k, has been calibrated (Butt and Jaschke 1995). For an extremely stiff sample, the deflection of the cantilever, d, is identical to the movement of the piezo scanner, z; however, for softer materials, the cantilever tip can indent the sample. The indentation, δ, reduces the total deflection, $d = z\text{-}\delta$, and the loading force is now given by $F = kd = k(z - \delta)$. A modified Hertz model is used to describe the elastic deformation of the sample by relating the indentation and loading force (Hertz 1881, Sneddon 1965). For a conical tip pushing onto a flat sample, the force is given by:

$$F = \frac{2}{\pi}\tan(\alpha)\frac{E}{1-\nu^2}\delta^2 \tag{1.17}$$

where α is the half-opening angle of the AFM cone-tip, E is the Young's modulus, and ν is the Poisson ratio of the sample. By combining the above equations we obtain:

$$z - z_o = d - d_o + \sqrt{\frac{k(d-d_o)}{(2/\pi)[E/(1-\nu^2)]\tan(\alpha)}} \tag{1.18}$$

where d_o is the zero deflection position and is determined from the non-contact part of the force-curve, and z_o is the contact point. Typically, ν is assumed or measured independently and the force curve is fit to determine E and z_o. There are two common sources of measurement error. For very soft samples, it is difficult to determine the exact point of contact, leading to uncertainty in the measurement of E. Also, for very thin or soft materials, the elastic response of the underlying hard substrate that supports the soft sample can contribute; in this case, the measured value of E should be taken as an upper bound. The contribution of the rigid substrate is greater for higher forces and indentations, and can be reduced by attaching a colloidal particle to the conical tip. With a spherical tip, the contact area is increased, allowing the same stress to be applied to the sample with a smaller force. Moreover, using a range of sizes of colloidal particles, the applied stress can be varied in a controlled manner; the applied stress is typically 100 – 10000 Pa for colloids of ranging in size from less than 1 μm to 12 μm in diameter (Mahaffy et. al. 2000). For a spherical tip of radius R, the modified Hertz model predicts:

$$F = \frac{4E\sqrt{R}}{3(1-\nu)}\delta^{3/2} \tag{1.19}$$

Another related technique, called Force Integration to Equal Limits (FIEL), allows the mapping of relative micro-elastic response in systems with spatial inhomogeneities or dynamic re-arrangements (A-Hassan, et al. 1998). This technique has several advantages over traditional analysis since the relative elastic map is independent of the tip-sample contact point and the cantilever spring constant. In FIEL, a pair of force-curves is collected at two different positions in the sample in constant force mode, imposing the condition that F_1=F_2 where the subscript distinguishes the two measurements. For a spherical tip geometry, the force balance gives:

$$\frac{4}{3}\frac{\sqrt{R}}{\pi k_1}\delta_1^{3/2} = \frac{4}{3}\frac{\sqrt{R}}{\pi k_2}\delta_2^{3/2} \tag{1.20}$$

where k is the local spring constant of the sample is the defined as: $k = 1-\nu/\pi E$. This equation reduces to:

$$\left(\frac{\delta_1}{\delta_2}\right)^{3/2} = \frac{k_1}{k_2} \tag{1.21}$$

The work done by the AFM cantilever during indentation can be calculated by integrating the force-curve over the indentation depth:

$$w_i = \int_0^{\delta_i} \frac{4}{3}\frac{\sqrt{R}}{\pi k_i}\delta_i^{3/2} d\delta = \frac{8}{15}\frac{\sqrt{R}}{\pi k_i}\delta_i^{5/2} \tag{1.22}$$

where the index *i* indicates a single force-curve measurement. The relative work done is given by the ratio of work done in each measurement:

$$\frac{w_1}{w_2} = \left(\frac{\delta_1}{\delta_2}\right)^{5/2}\frac{k_2}{k_1} . \tag{1.23}$$

Combining the two above equations, we obtain an expression for the relative local elasticity, given by:

$$\frac{w_1}{w_2} = \left(\frac{k_1}{k_2}\right)^{2/3} . \tag{1.24}$$

This approach works for other tip geometries as well, with a change only in the scaling exponent; the exponent is 2/3 for a spherical or parabolic tip, 1/2 for a conical tip, and one for a flat-end cylinder. By comparing many force curves obtained at many different locations in the sample, a map of relative microelasticity across the surface is obtained. If the same probe is used in all measurements, the result is independent of the exact probe size, cantilever spring constant, and deflection drift. This method is independent of sample topography and does not require absolute height measurements. FIEL mapping is most useful for measuring relative changes in elasticity in dynamic systems and is not appropriate for measuring absolute moduli. In order to obtain absolute measures of elasticity and to compare FIEL maps obtained with different cantilevers, additional calibration procedures are necessary.

In viscoelastic samples, AFM techniques can be modified to measure viscosity and the frequency dependent response. Qualitative measures of the viscosity are possible by measuring the relaxation of the tip into the sample or the hysteresis of the force-curves. For more precise and frequency-dependent measurements, an oscillating cantilever tip can be used (A-Hassan, et al. 1998, Mahaffy, et al. 2000). A small amplitude sinusoidal signal, $\tilde{\delta}$, typically 5-20

nm, is applied normal to the surface around the initial indentation, δ_o, at frequencies in the range of 20-400 Hz. A lock-in amplifier is used to measure the phase and amplitude of the response with respect to the driving force. The modified Hertz model must now include a frequency dependent response term, and for small oscillations the force is given by:

$$f_{bead} \approx \frac{4}{3}\sqrt{R}\left(\bar{E}_o \delta^{3/2} + \frac{3}{2}\bar{E}^* \sqrt{\delta_o}\tilde{\delta} \right) \tag{1.25}$$

where $\bar{E}^*$ is analogous to the complex shear modulus, G^*, and is defined as the frequency-dependent part of the constant ratio $E/(1-\nu^2)$:

$$\bar{E}^* \equiv \frac{E}{1-\nu^2} = \frac{2(1+\nu)}{(1-\nu^2)G^*} \tag{1.26}$$

and $\bar{E}_o$ refers to the zero-frequency value of $\bar{E}^*$ defined as:

$$\bar{E}_o \equiv \frac{2(1+\nu)}{(1-\nu^2)G'(0)} \tag{1.27}$$

where $G'(0)$ is the real part of the complex shear modulus, the elastic modulus, at zero frequency. The second term in the modified Hertz model describes the time-dependent response and includes contributions of both the viscous drag force on the cantilever as it oscillates in the surrounding fluid and the viscoelastic response of the substrate. The viscous force on the cantilever is dependent on the frequency of oscillation and is given by:

$$f_{drag} = i\omega\alpha\tilde{\delta} \tag{1.28}$$

where ω is oscillation frequency, and α is a constant that includes the driving amplitude, the viscosity of the fluid, and the geometry of the cantilever. This contribution must be subtracted from the time-dependent response in order to measure the frequency dependent viscoelastic moduli, which depend only on the material properties of the soft substrate.

AFM techniques allow measurements of elastic or viscoelastic response of thin samples and surfaces. Images are often obtained simultaneously, allowing mechanical properties to be correlated with local topography and microstructure. Relative elastic mapping and fast AFM scans allow measurements of the dy-

namic changes in mechanics or structure. As in all active manipulation techniques, the strain amplitude and driving frequency can be varied and out-of-equilibrium measurements are possible.

1.3 Passive Microrheology Methods

A second class of microrheology techniques uses the Brownian dynamics of embedded colloids to measure the rheology and structure of a material. Unlike *active* microrheology techniques that measure the response of a probe particle to an external driving force, *passive* measurements use only the thermal energy of embedded colloids, determined by k_BT, to measure rheological properties. For passive measurements, materials must be sufficiently soft in order for embedded colloids to move detectably with only k_BT of energy. The thermal motion of the probe in a homogeneous elastic medium depends on the stiffness of the local microenvironment. Equating the thermal energy density of a bead of radius a to the elastic energy needed to deform a material with an elastic modulus G' a length L yields:

$$\frac{k_BT}{a^3} = \frac{G'L^2}{a^2} \quad . \tag{1.29}$$

For most soft materials, the temperature cannot be changed significantly. Thus, the upper limit of elastic modulus we are able to measure with passive techniques depends on both the size of the embedded probe and on our ability to resolve small particle displacements of order L. The resolution of detecting particle centers depends on the particular detection scheme used and typically ranges from 1 Å to 10 nm, allowing measurements with micron-sized particles of samples with an elastic modulus up to 10 to 500 Pa. This range is smaller than that accessible by active measurements, but is sufficient to study many soft materials. Moreover, passive measurements share the distinct advantage that results are always within the linear viscoelastic regime because there is no external stress applied.

To understand how the stochastic thermal energy of embedded micron-sized particles is used to probe the frequency dependent rheology of the surrounding viscoelastic material, it is useful to first consider the motion of spheres in a purely viscous fluid then generalize to account for elasticity. Micron-sized spheres in a purely viscous medium undergo simple diffusion, or Brownian motion. The dynamics of particle motions are revealed in the time dependent position correlation function of individual tracers. This correlation function, also known as the mean squared displacement (MSD), is defined as:

$$\left\langle \Delta\vec{x}^2(\tau)\right\rangle = \left\langle \left|\vec{x}(t+\tau)-\vec{x}(t)\right|^2 \right\rangle_t \tag{1.30}$$

where $\vec{x}$ is the *d*-dimensional particle position, τ is the lag time and the brackets indicate an average over all times *t*. The time-average assumes the fluid is in always in thermal equilibrium and the material properties do not evolve in time. The diffusion coefficient, *D*, of the Brownian particles is obtained from the diffusion equation:

$$\left\langle \Delta\vec{x}^2(\tau)\right\rangle = 2dD\tau \tag{1.31}$$

From this, the viscosity η of the fluid surrounding the beads of radius *a* is obtained using the Stokes-Einstein equation: $D = k_BT / 6\pi\eta a$ (Reif 1965).

Many materials are more complex, exhibiting both viscous and elastic behavior. Additionally, the responses are typically frequency dependent and depend on the time and length scale probed by the measurement. For such materials, the thermally driven motion of embedded spheres reflects both the viscous and elastic contributions, which are revealed in the MSDs of the tracers (Mason and Weitz 1995). Unlike a simple fluid where the MSDs of embedded tracers evolve linearly with time, the MSDs of tracers in a complex material may scale differently with τ,

$$\left\langle \Delta\vec{x}^2(\tau)\right\rangle \sim \tau^{\alpha} \tag{1.32}$$

where α<1 and is called the diffusive exponent. The particles may exhibit subdiffusive motion (0<α<1) or become locally constrained (α = 0) at long times.

In the case of a pure elastic homogenous material, a plateau in the MSD occurs when the thermal energy density of the bead equals the elastic energy density of the network that is deformed by the displacement of the bead:

$$\left\langle \Delta x^2\left(\tau\to\infty\right)\right\rangle = \frac{k_BT}{\pi G'a} \tag{1.33}$$

Analogous to a harmonic oscillator, the elastic energy of deformation of a material can be understood as the energy of a spring with a spring constant proportional to $G'a$. The energy of the spring is simply the thermal energy, k_BT. A viscoelastic material can be modeled as an elastic network that is viscously coupled to and embedded in an incompressible Newtonian fluid (Levine and Lubensky 2000). A natural way to incorporate the elastic response is to generalize the standard Stokes-Einstein equation for a simple, purely viscous fluid with a com-

plex shear modulus $G(\omega)= i\omega\eta$ to materials that also have a real component of the shear modulus. A generalized Langevin equation is used to describe the forces on a small thermal particle of mass m and velocity $v(t)$ in a complex material:

$$m\dot{v}(t) = f_R(t) - \int_0^t \zeta(t-\tau)v(\tau)d\tau \tag{1.34}$$

where $f_R(t)$ represents all the forces acting on the particle, including both the interparticle forces and stochastic Brownian forces. The integral represents the viscous damping of the fluid with a time dependent memory function $\zeta(t)$ to account for the elasticity in the network. By taking the unilateral Laplace transform of the generalized Langevin equation and using the equipartition theorem, the viscoelastic memory function can be related to the velocity autocorrelation function (Mason, et al. 1997):

$$\langle v(s)v(0)\rangle = \frac{k_B T}{ms - \zeta(s)} \tag{1.35}$$

where s represents frequency in the Laplace domain. The inertial term is negligible except at very high (~ MHz) frequencies (Levine and Lubensky 2000). When the velocity autocorrelation is written in terms of the Laplace transform of MSD, the expression for the memory function in Laplace space becomes

$$\tilde{\zeta}(s) = \frac{6k_B T}{s^2 \langle \Delta\tilde{r}^2(s)\rangle}. \tag{1.36}$$

To relate the microscopic memory function to the bulk viscoelasticity, the Stokes law is generalized to include a frequency dependent complex viscosity (Mason and Weitz 1995). In the Laplace domain, this relates the complex shear modulus $\tilde{G}(s)$ to the memory function $\tilde{\zeta}(s)$ as

$$\tilde{G}(s) = \frac{s\tilde{\zeta}(s)}{6\pi a}. \tag{1.37}$$

By combining these two equations, we obtain a relationship that directly relates the mean-squared displacement of the tracers to the bulk modulus of the material:

$$\tilde{G}(s) = \frac{k_B T}{\pi a s \left\langle \Delta \tilde{r}^2(s) \right\rangle} \quad (1.38)$$

This equation is a generalized, frequency-dependent form of the Stokes-Einstein equation for complex fluids. In the limit of a freely diffusing particle in a purely viscous solution,

$$\left\langle \Delta \tilde{r}^2(s) \right\rangle = 6D / s^2 \quad (1.39)$$

and the generalized Stokes-Einstein relation (GSER) recovers the frequency independent viscosity, $\eta_0 = k_B T / 6\pi a D$, where D is the diffusion coefficient of the particle in the fluid. This result of the generalized Stokes-Einstein equation is remarkable: simply by observing the time-evolution of the MSD of thermal tracers, we obtain the linear, frequency dependent viscoelastic response.

To compare with bulk rheology measurements, $\tilde{G}(s)$ is transformed into the Fourier domain to obtain $G^*(\omega)$. $G^*(\omega)$ is the complex shear modulus and is the same quantity measured with a conventional mechanical rheometer. $G^*(\omega)$ can be written as the sum of real and imaginary components: $G^*(\omega) = G'(\omega) + iG''(\omega)$. Since $G'(\omega)$ and $G''(\omega)$ are not independent and obey Kramers-Kronig relations, it is possible to determine both from the single, real function $\tilde{G}(s)$. This can be done, in principle, by calculating the inverse unilateral Laplace transform and then taking the Fourier transform (Schnurr, et al. 1997).

Equivalently, an alternative expression for the GSER can be written in the Fourier domain as:

$$G^*(\omega) = \frac{k_B T}{\pi a i\omega \Im_u \left\langle \Delta r^2(t) \right\rangle} \quad (1.40)$$

A unilateral Fourier transform, $\Im_u$, is effectively a Laplace transform generalized for a complex frequency $s=i\omega$. In practice, the numerical implementation of this process for discretely sampled data of $<\Delta r^2(t)>$ over a limited range of times can cause significant errors in $G^*(\omega)$ near the frequency extremes. Alternatively, a local power law expansion of $<\Delta r^2(t)>$ can be used to derive algebraic estimates for $\tilde{G}(s)$ and $G^*(\omega)$ (Mason, et al. 1997, Dasgupta, et al. 2001). This approximation is discussed in the Appendix.

To use the generalized Stokes-Einstein relation to obtain the macroscopic viscoelastic shear moduli of a material, it is necessary that the medium around the sphere may be treated as a continuum material. This requires that the size of bead be larger than any structural length scales of the material. For example, in a polymer network, the size of the bead should be significantly larger than the characteristic mesh size.

Recent theoretical work has shown that the GSER describes the thermal response of a bead embedded in a viscoelastic medium within a certain frequency range, $\omega_B < \omega < \omega^*$ (Levine and Lubensky 2000). The lower limit, ω_B, is the time scale at which longitudinal, or compressional, modes become significant compared to the shear modes that are excited in the system. In bulk rheology, the applied strain has only a shear component, but the thermally driven probe particle responds to all of the thermally excited modes of the system including the longitudinal modes of the elastic network. At frequencies lower than ω_B, the network compresses and the surrounding fluid drains from denser parts of the network. Above ω_B, the elastic network is coupled with the incompressible fluid and longitudinal modes of the network are suppressed. In this regime, the probe motion is entirely due to excited shear modes of the material (Schnurr, et al. 1997). An estimate of the lower crossover frequency, ω_B, can be determined by balancing local viscous and elastic forces. The viscous force per volume exerted by the solvent on the network is $\sim \eta v / \xi^2$, where v is the velocity of the fluid relative to the network, η is the viscosity of the fluid and ξ is the characteristic length scale of the elastic network. The local elastic force per volume exerted by the network is $G'\nabla^2 u \sim G'u / a^2$ at the bead surface where u is the network displacement field and a is the radius of the bead. Viscous coupling will then dominate above a crossover frequency

$$\omega_B \geq \frac{G'\xi^2}{\eta a^2}. \tag{1.41}$$

For a typical soft material with an elastic modulus of 1 Pa, viscosity of 0.001 Pa*sec and a mesh size one-tenth the radius of embedded probe, this crossover frequency ω_B is approximately 10 Hz.

The upper frequency limit, ω^*, exists due to the onset of inertial effects of the material at the length scale of the bead. Shear waves propagated by the motion of the tracer decay exponentially from the surface of the bead through the surrounding medium. The characteristic length scale of decay is called the viscous penetration depth and is proportional to $\sqrt{G^* / \rho\omega^2}$ where ρ is the density of the surrounding fluid and ω is the frequency of the shear wave (Ferry 1980). The viscous penetration depth sets a length scale for how far information is propagated in the medium when probed with a shear strain at a certain frequency

ω. When the magnitude of the viscous penetration depth equals the size of the bead, inertial terms cannot be neglected. For a typical soft material, inertial effects can be expected to be significant only for frequencies larger than 1MHz (Schnurr, et al. 1997).

From these analyses, we find in typical experiments there is a very large frequency range 10 Hz < ω < 100 kHz where the generalized Stokes-Einstein equation is accurate and valid. Note that this is much higher than traditional mechanical measurements where inertial effects begin to become significant around 50 Hz. Additionally, models have been proposed for the frequency regimes where the GSER does not hold (Levine and Lubensky 2000).

To take full advantage of the range of frequencies and complex moduli accessible in a passive microrheology experiment, it is necessary to use techniques that measure the mean-squared displacement (MSD) of embedded spheres with excellent temporal and spatial resolution. The MSD can be calculated from methods that directly track the particle position as a function of time or can be obtained from ensemble-averaged light scattering experiments. Methods of particle detection vary significantly in temporal and spatial resolution, affecting the types of measurement possible with each technique. Additionally, techniques differ significantly in their ability to provide statistical accuracy over an ensemble of probes.

Particle tracking methods have been developed to directly image the position of a colloidal sphere as a function of time. Because the entire particle trajectory is directly obtained, these techniques allow further analysis of individual trajectories beyond an ensemble averaged MSD. These analyses often provide further insight into the local structures and rheology of the surrounding medium. Methods of particle tracking differ in the spatial and temporal resolution of the particle trajectories. The temporal resolution is determined by the frequency at which particle positions can be recorded. The spatial resolution is determined by how precisely differences in the particle position are measured. This, in turn, is used to determine an upper bound on the elastic modulus that can be detected using thermal motion with a given experimental technique.

The motion of individual tracers can be measured with laser detection schemes nearly identical to the optical tweezers setup described in Section 1.2.2 (Mason, et al. 1997, Schnurr, et al. 1997). Unlike optical tweezers, the laser power used in laser deflection particle tracking is quite low so that the optical forces are very small (< 5%) compared to the thermally driven forces of the bead. The thermally driven motion will cause the bead to move off the beam's axis and deflection of the laser beam can be measured. From this deflection, the displacement of the single bead is detected from which the MSD (Mason, et al. 1997) or the power spectral density (Schnurr, et al. 1997), the position correlation function in frequency space, can be calculated. The power spectral density of the beads is interpreted as the viscoelastic response of the material in a similar manner as the MSD (Schnurr, et al. 1997). This detection scheme has excellent

spatiotemporal resolution; individual particles are tracked with subnanometer precision at frequencies up to 50 kHz. The enhanced frequency regime allows study of rheology of polymer networks at time scales where single filament properties often dominate the rheological response. However, this technique is limited in its statistical accuracy in two ways. First, it is somewhat difficult to obtain particle trajectories for a large ensemble of beads as this requires many consecutive measurements of individual beads. Secondly, in practice, it is difficult to track a single bead with this technique for longer than a few minutes because freely moving particles can diffuse out of the beam. While this track length is more than sufficient for the higher end of the frequency sweep, the low frequency statistics are limited. This strength of this technique resides in its ability to detect extremely small displacements of individual beads at high frequencies inaccessible to other video-based methods. Laser Deflection Particle Tracking has been used to study the rheology of F-Actin networks (Gittes, et al. 1997, McGrath, et al. 2000, Tseng and Wirtz 2001) and living cells (Yamada, et al. 2000).

Alternatively, it is possible to directly image the embedded beads using a simple video microscopy setup. Video microscopy of single beads is often used in active measurements as well, in particular with the magnetic bead microrheology experiments discussed in Section 1.2.1. Techniques in image processing have been developed to automate the process of accurate particle center location to simultaneously track hundreds of embedded probes in a single field of view of the microscope with submicron precision. While video microscopy is limited to frequencies available to the camera, the strength of the technique is in its ability to obtain good statistics on ensembles of beads.

Embedded spheres are imaged with a conventional light microscope using either fluorescence or bright field microscopy. Using bright field microscopy, spheres larger than a few hundred nanometers can be observed but the diffraction limited resolving power of the microscope precludes the study of smaller probes. Fluorescent labeling offers the ability to observe smaller probes, which now act as point sources of light, as well as the opportunity to perform colocalization studies with differently dyed beads. Fluorescently labeled colloidal spheres are commercially available from 20 nm up to several microns.

In a typical video based experiment, a time series of microscope images is obtained with a CCD camera and recorded in analog format onto a S-VHS cassette using commercially available video tape recorders. Video images are digitized using a computer equipped with a frame grabber card. Until recently, it was not possible to write a full frame image of 480 x 640 pixels directly to the hard drive at the standard video rates of 30 Hz due to limitations in the speed at which information can be transferred. With advances in computer technology, it is now possible to write full frame images directly to the hard drive at 30 Hz (Keller, Schilling et al. 2001); nonetheless, capturing movies to videotape affords the ability to store large amounts of data conveniently.

Of some concern is that the frequency ranges for video microscopy are around 10 Hz, earlier estimated as the lower frequency limit of the generalized Stokes-Einstein relation (GSER). This frequency limit is simply an estimate for when compressibility effects may become significant in a viscoelastic medium and preclude the use of the GSER. However, this lower frequency limit varies widely in different samples. Some materials, like simple fluids, are known to be incompressible at all frequencies. Additionally, in Section 1.5, formalism will be introduced to test for and even quantify compressibility effects using particle tracking with a video microscopy apparatus.

In a homogeneous, isotropic material, it is sufficient to examine the projection of the particle trajectory along a single axis. In heterogeneous materials, it may be useful to be able to obtain two- or three-dimensional particle trajectory. In video microscopy, the motion of the particle is projected into the plane of the focus and a two dimensional trajectory is obtained for further analysis. Techniques have been developed to track particles in the direction perpendicular to the plane of focus either by modifying the optics in a conventional microscope (Kao and Verkman 1994) or by carefully examining the structure of the Airy disk created by circular particles in bright field microscopy (Kao and Verkman 1994, Ovryn 2000, Ovryn and Izen 2000). However, confocal microscopy is currently most widely used to follow the three dimensional motion of fluorescently tagged colloids (Weeks, et al. 2000, Dinsmore, et al. 2001).

The power in using video microscopy for microrheology lies in the potential of following the motions of roughly a hundred colloidal particles simultaneously and the ability to obtain the ensemble averaged mean-squared displacement (MSD) while still retaining each of the individual particle trajectories. The ability to accurately and precisely find the centers of the two-dimensional colloidal images in each frame of video is crucial. Algorithms have been developed to automate the process of finding particle centers and accurately find particles to roughly 1/10 of a pixel, and are described in the Appendix (Crocker and Grier 1996). For a typical magnification, this is a resolution of 10 nm. Once colloidal particles are located in a sequence of video images, particle positions in each image are correlated with positions in later images to produce trajectories. To track more than one particle, care is required to uniquely identify each particle in each frame (Crocker and Grier 1996).

Multiparticle tracking is particularly well suited to study materials that are heterogeneous at the length scales of the bead; for these systems, single bead measurements are not sufficient to describe a bulk response, but particle movements do reveal details of the local mechanics and microstructure. Measurements on heterogeneous materials will be discussed in Section 1.4. In the case of homogeneous materials, each thermally activated particle measures the same continuum viscoelastic response; as a result, measurements on ensembles of particles are often preferable to single bead measurements by providing better statistical accuracy in calculating the MSD and moduli. Ensemble averaged behaviors can be obtained by averaging many single particle motions that are

simultaneously obtained with video microscopy; however, light scattering techniques are often preferable. Light scattering methods inherently average over a large ensemble of particles, and are not appropriate for samples that may exhibit local heterogeneity; however, for homogeneous samples, light scattering has the advantage of better averaging and statistical accuracy and a larger accessible frequency range than any macroscopic measurement or video-based microrheology technique.

In a typical dynamic light scattering measurement, a laser beam impinges on a sample and is scattered by the particles into a detector placed at an angle, θ, with respect to the incoming beam (Berne and Pecora 2000). As the particles diffuse and rearrange in the sample, the intensity of light that reaches the detector fluctuates in time. In the simplest case, each photon is scattered only once within the illumination volume directly into the detector. The intensity fluctuations are measured as a function of time, $I(t)$, and the normalized intensity correlation function, $g_2(\tau)$, is calculated:

$$g_2(\tau) = \frac{\langle I(t)I(t+\tau)\rangle}{\langle I(t)\rangle^2} \tag{1.42}$$

where the brackets indicate an average over time. The measured g_2, can be related to the calculated field correlation function, g_1, which is given by:

$$g_1(\tau) = \frac{\langle E(t)E^*(t+\tau)\rangle}{\langle |E(t)|\rangle^2} \tag{1.43}$$

where E is the scattered electric field, using the Siegert relation:

$$g_2(\tau) = 1 + \beta |g_1|^2 \tag{1.44}$$

where β is determined by the coherence of the detection scheme. For measurements of a single coherence area, or speckle, $\beta \approx 1$. If all particles are statistically independent, and moving randomly due to thermal impulses only, then:

$$g_1(\tau) = \exp[-q^2 \langle \Delta r^2(\tau)\rangle / 6] \tag{1.45}$$

where $\left\langle \Delta r^2(\tau) \right\rangle$ is the ensemble averaged three-dimensional MSD, and q is the scattering wave vector given by:

$$q = \frac{4\pi n}{\lambda} \sin\left(\frac{\theta}{2}\right) \tag{1.46}$$

where n is the index of refraction of the sample and λ is the wavelength of the laser *in vacuuo*. The correlation function decays as the scatters move a distance $1/q$. For some elastic samples, particles may be locally constrained and unable to move $1/q$ during the measurement, leading to "non-ergodic" behavior. In order to extract the ensemble average of the field correlation function from the measured time-averaged intensity fluctuations, a different method of analysis is required (Pusey and van Megen, 1989, Joosten et. al. 1990, van Megen et. al. 1991, Xue et. al. 1992). Once the MSD is obtained, the generalized Stokes-Einstein formalism can be applied to extract the frequency dependent viscoelastic moduli. Single light scattering techniques are typically sensitive to frequencies in the range of 0.01 – 10 Hz, similar to the frequency range available with a conventional macroscopic rheometer.

A second light scattering technique, Diffusing Wave Spectroscopy (DWS), allows measurements of multiple scattering media and extends the accessible frequency range to much higher frequencies (Pine, et al. 1988, Weitz and Pine 1993). The experimental set-up is similar to that of the single-scattering experiment; however, in this case, a laser beam impinges on an opaque sample and the light is scattered multiple times before exiting. The diffusion equation is used to describe the propagation of light through the sample. All q-dependent information is lost as the photons average over all possible angles, resulting in only two experimental geometries: transmission and backscattering. Like single scattering experiments, the intensity of a single coherence area is detected; fluctuations in intensity reflect the dynamics of the scattering medium and the mean squared displacement of the particles can be obtained. The field correlation function can be expressed as:

$$g_1(\tau) \propto \int_0^\infty P(s) \exp\left[-\frac{k_o^2 s \left\langle \Delta r^2(\tau) \right\rangle}{3l^*} \right] ds \tag{1.47}$$

where $P(s)$ is the probability of light traveling a path length s, and is determined by solving the diffusion equation with the experimental boundary conditions, $k_o = 2\pi n/\lambda$ where n is the index of refraction of the solution, λ is the wavelength of light *in vacuuo*, and l^* is transport mean free path and is defined as the distance the light must travel before its direction is completely randomized. The mean

free path is determined in an independent measurement of the transmitted intensity and is typically much smaller than the thickness of the sample chamber. The correlation function decays when the total path length of the light through the sample changes by roughly the wavelength of the incident beam. To achieve this, each particle in the path of the light needs to move only a fraction of a wavelength; as a result, DWS is sensitive to motions on much smaller length scales and faster time scales than single scattering measurements. Analytic inversion is used to obtain the MSD from $g_1(\tau)$. The typical frequency range in a DWS measurement is $10 - 10^5$ Hz, allowing direct measurements of the high-frequency response of polymer solutions and other materials that are impossible with traditional mechanical measurements. The microrheology of flexible and semi-flexible polymer solutions has been measured using light scattering techniques (Mason, et al. 1996, Mason, et al. 1997, Gisler and Weitz 1998, Gisler and Weitz 1999, Palmer, et al. 1999, Mason, et al. 2000, Dasgupta, et al. 2001).

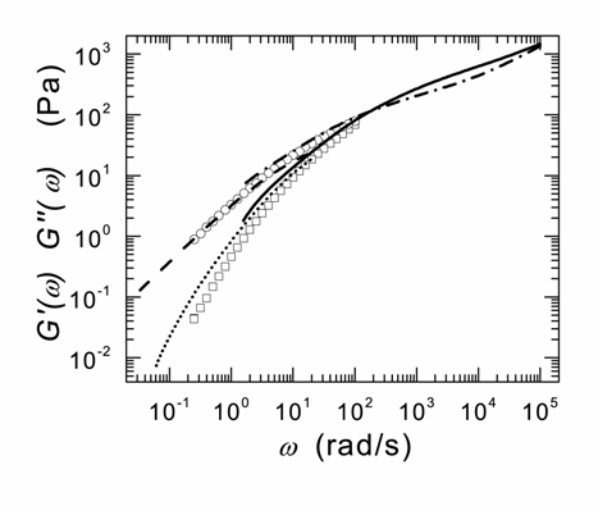

Fig. 1.5. The storage and loss moduli obtained by Dasgupta et al. (Dasgupta, et. al. 2001) for a 4% by weight 900 kDa PEO solution comparing moduli obtained with a conventional strain controlled rheometer (G' – open square, G" – open circle) to those obtained by both DWS (G' – solid line, G" – dash-dot) and single scattering at 20o (G'- dot, G" – dash). The beads used in both light scattering techniques are 0.65 micron spheres. Using the three techniques, it is possible to obtain data over ~6 decades in frequency. Additionally, the moduli obtained via light scattering are in excellent agreement with bulk measurement. Similar agreement between DWS and bulk rheology was found for other concentrations of PEO as well. (reprinted with permission from Dasgupta et al. 2001)

As seen in Fig. 1.5, Dasgupta et al. have demonstrated excellent agreement between moduli obtained for a flexible polymer solution, polyethylene oxide (PEO), using DWS and single light scattering microrheology and mechanical rheometry.

1.4 Practical Applications of One-Particle Microrheology

Because the techniques discussed in Sections 1.2 and 1.3 interpret the dynamics of individual probe particles as a viscoelastic response, these techniques have come to be known as one-particle microrheology. One-particle microrheology is a powerful tool to study the rheological properties of samples with extremely small sample volumes at frequencies inaccessible to bulk measurements. The development of microrheological techniques is currently an active field and the full range of possibilities, and limitations, of microrheology tools has yet to be completely understood. Here we discuss important issues to consider before interpreting the individual bead motion as a bulk rheological response of the material.

One-particle microrheology assumes the local environment of the bead reflects that of the bulk. If the surface chemistry of the bead modifies the structure of the material around the bead, the one-particle response will be a reflection of the local microenvironment rather than bulk rheology. Interactions between the embedded probe and sample are of much interest and are highly system dependent. In studies with polyethylene oxide, an uncross-linked flexible polymer solution, there is no effect of bead chemistry (Dasgupta, et al. 2001). However, surface chemistry seems to have significant effects with biopolymer networks (McGrath, et al. 2000). The charge groups used to stabilize commercially available colloids are reactive with many proteins, leading to unspecific binding. In a careful study with F-actin networks, the bead chemistry was changed to either inhibit or to encourage binding of actin to the bead surface (McGrath, et al. 2000). The beads that prevented actin binding were insensitive to changes in the mechanical properties of the network. By contrast, beads that bound to actin filaments reflected the bulk properties of the networks more accurately. However, it is often difficult to precisely control protein adsorption onto the beads. Moreover, although in some cases binding helps one-particle microrheology probe bulk properties, there may be other consequences. In the worst-case scenario, there is significant aggregation of the probes and the macroscopic gel-like structures are significantly altered. In less extreme cases, the presence of the bead affects only the surrounding local network but the bulk properties are unchanged. In this case, it is possible to obtain a modulus from one-particle microrheology but it is unclear whether the measured local modulus reports the bulk response.

In general, it is advisable to test for probe surface chemistry effects in a new system. In Section 1.5, two-particle microrheology will be discussed. Unlike one-particle microrheology that measures individual bead response to the surrounding microenvironment, two-particle microrheology is independent of bead surface chemistry.

One-particle microrheology has the additional feature that bulk response is measured only if the probe size is larger than the length scale of heterogeneity in the sample. These length scales are often unknown prior to a microrheology experiment. When the particle diameter is comparable to or smaller than the length scale of structures in the medium, the tracers can move within small cavities and their motions are not only a measure of the viscoelastic response, but also of the effect of steric hindrances caused by the cavity walls (Valentine, et al. 2001). A material like agarose is a prime example. Agarose is known to be structurally heterogeneous and consists of a network of fibrous molecules. The elastic modulus of agarose, as measured in a bulk rheometer, is roughly 2700 Pa and too high to measure with a passive microrheological technique. However, while agarose contains large elastic structures that span the sample and bear macroscopic stress, these structures do not form a homogeneous elastic medium. Instead, agarose is characterized by many smaller voids, or pores, through which smaller particles may move. By observing the dynamics of smaller particles within the pores, one is actually characterizing the structural and mechanical properties of the weaker pores rather than the bulk continuum properties.

In a particle tracking experiment, a plateau in the ensemble averaged mean-squared displacement at long lag times, $<\Delta x^2(\tau \to \infty)>$, indicates that the particles are constrained by the material, but it is necessary to examine how this plateau varies with particle radius, a, to determine the nature of the constraint. If the plateau is a measure of local elasticity G then $<\Delta x^2(\tau \to \infty)> = kT/\pi Ga$, so $<\Delta x^2(\tau \to \infty)>$ scales with $1/a$. If the plateau is a measure of a pore size d then $d=a+h$ where h is the size of the fluid filled gap between the particle and the pore wall and can be approximated by $h=<\Delta x^2(\tau \to \infty)>^{1/2}$. Thus, if the particle is measuring a purely steric boundary then $a+<\Delta x^2(\tau \to \infty)>^{1/2}$ remains roughly constant. It is important to test trends in mean-squared displacement as a function of bead size to determine the nature of the constraints felt by the bead. The technique of two-particle microrheology is able to distinguish between measurement of a steric boundary and a local modulus.

In heterogeneous materials, individual particles movements must be considered since different particles may be exploring different microenvironments. Statistical techniques have been developed to compare the individual particles and map spatial and temporal variation in mechanical response (Valentine et al. 2001). Furthermore, particles in similar microenvironments can be grouped together into a meaningful ensemble and average rheological and structural properties can be obtained.

1.5 Two-Particle Microrheology

One-particle microrheology is very sensitive to the local environment of the embedded bead. If the tracers locally modify the structure of the medium or sample only the weak pores in a heterogeneous material, then one-particle microrheology determines the structure and mechanics of the local microenvironment rather than bulk rheology. The recently developed technique of two-particle microrheology (Crocker, et al. 2000) eliminates motion due to purely local structure and mechanics by measuring the cross-correlated motion of pairs of tracer particles within the sample. The correlated motion of the particles is not affected by the size, or even shape, of the tracer particles and is independent of the specific coupling between the probe and the medium. Furthermore, the length scale being probed is not the individual bead radius, a, but is the distance, r, between the tracers which is typically 10-100 microns rather than 1 micron. This increase in length scale means that the technique is insensitive to short wavelength heterogeneities in the sample smaller than the bead separation distance and thus may probe bulk rheology even if individual particles do not. Additionally, probing longer length scales lowers the frequency limit, ω_B, of the generalized Stokes-Einstein equation by replacing a by r in Eqn. 1.40. Two-particle microrheology directly maps the long-range deformation or flow of the material due to a single tracer's motion. Since one tracer's strain field will entrain a second particle, the cross-correlated motion of two tracers' movements is a direct map of the strain field in the material. In a medium that is homogeneous at long length scales and characterized by a bulk viscoelasticity, the strain field is proportional to the tracer motion and decays like a/r where r is the distance from the tracer. Local heterogeneities either intrinsic to the material or created by the presence of the probe will affect individual particle motions but the movements will be uncorrelated at large distances.

With modifications, a two-particle measurement is possible with most of the active and passive techniques previously discussed. Video based multiparticle tracking is particularly well suited to examine cross-correlated motion because several hundred tracers can be imaged simultaneously (Crocker, et al. 2000). In a typical two-particle measurement, roughly one hundred tracers are observed for several hundred seconds at video rate to gather sufficient statistics. Vector displacements of individual tracers are calculated as a function of lag time, τ, and absolute time, t: $\Delta r_\alpha(t,\tau) = r_\alpha(t+\tau) - r_\alpha(t)$. Then the ensemble averaged tensor product of the vector displacements is calculated:

$$D_{\alpha\beta}(r,\tau) = \left\langle \Delta r_\alpha^i(t,\tau)\Delta r_\beta^j(t,\tau)\delta\left[r - R^{ij}(t)\right]\right\rangle_{i\neq j,t} \tag{1.48}$$

where i and j label two particles, α and β are coordinate axes and R^{ij} is the distance between particles i and j. The average is taken over the only the distinct terms ($i \neq j$); the "self" term yields the one-particle mean-squared displacement, $<\Delta r^2(\tau)>$.

The two-particle correlation for particles in an incompressible continuum is calculated by treating each thermal particle as a point stress source and mapping its expected strain field (Landau and Lifshitz 1986). In the limit where the particle separation, r, is much greater than the particle radius a ($r >> a$), this is calculated by multiplying the one-particle mean-squared displacement predicted by conventional generalized Stokes-Einstein relation in (1.38) by a/r, to obtain:

$$\tilde{D}_{rr}(r,s) = \frac{k_B T}{2\pi r s \tilde{G}(s)}$$
$$D_{\theta\theta} = D_{\phi\phi} = \frac{1}{2} D_{rr} \tag{1.49}$$

where $\tilde{D}_{rr}(r,s)$ is the Laplace transform of $D_{rr}(r,t)$ and the off-diagonal terms vanish. While this result has been obtained for an incompressible medium, compressible materials can be treated by using a modifed Stokes-Einstein relation and strain field (Landau and Lifshitz 1986). The Brownian motion of a single probe is the superposition of all modes with wavelengths greater than the particle radius, a. The correlated motion of two tracers a separation r apart is driven only by modes with wavelengths greater than the separation distance. Therefore, two tracers that are separated by more than the coarse-grained length scale in an inhomogeneous medium will depend on the coarse-grained, macroscopic complex modulus. In an experiment, it is necessary to confirm that $\tilde{D}_{rr}(r,s) \sim 1/r$ by examining the correlated motion of at least several pairs of probes with different pairwise separations. If the strain field follows $1/r$ within a certain range of interparticle distances, the material can be treated as a homogeneous continuum at those length scales.

Comparing the longitudinal two-point correlation to the generalized Stokes-Einstein equation used in one-particle microrheology suggests defining a new quantity: the distinct mean-squared displacement, $<\Delta r^2(\tau)>_D$, as

$$\left\langle \Delta r^2(\tau) \right\rangle_D = \frac{2r}{a} \tilde{D}_{rr}(r,s) \tag{1.50}$$

This is the thermal motion obtained by extrapolating the long-wavelength thermal undulations of the medium to the bead radius. In a homogenous material where the GSER is valid, the distinct mean-squared displacement matches the

conventional one-particle mean-squared displacement. In inhomogeneous materials, differences between $<\Delta r^2(\tau)>_D$ and $<\Delta r^2(\tau)>$ provide insight into the local microenvironment experienced by the tracers. In this case, $<\Delta r^2(\tau)>$ may be understood as a superposition of a long-wavelength motion described by $<\Delta r^2(\tau)>_D$ plus a local motion in a cavity. Fig. 1.6a shows the comparison between the self and distinct mean squared displacements of 0.20 μm beads in a 0.25% guar solution. Guar is a naturally occurring neutral polysaccharide extracted from guar gum bean. A small concentration of guar in water dramatically changes the viscoelastic properties because of the formation of high-molecular weight, mesoscopic aggregates (Gittings, et al. 2000). Two-particle microrheology results are obtained by substituting $<\Delta r^2(\tau)>_D$ into the generalized Stokes-Einstein equation in place of $<\Delta r^2(\tau)>$. The self and distinct mean squared displacements results for the guar solution do not correspond, but disagree by a factor of two. In Fig. 1.6b, the data are converted into $G'(\omega)$ and $G''(\omega)$, and compared to results obtained from a macroscopic strain-controlled mechanical rheometer. As shown, the moduli calculated from the two-point correlation function are in good agreement with the results obtained with the rheometer. Single-particle microrheology provides qualitatively different moduli and completely fails to detect the crossover frequency. Unlike one-particle microrheology, two-particle microrheology is successful in determining the bulk rheological behavior of an inhomogeneous medium. This allows measurements in a larger range of materials than previously accessible with one-particle microrheology.

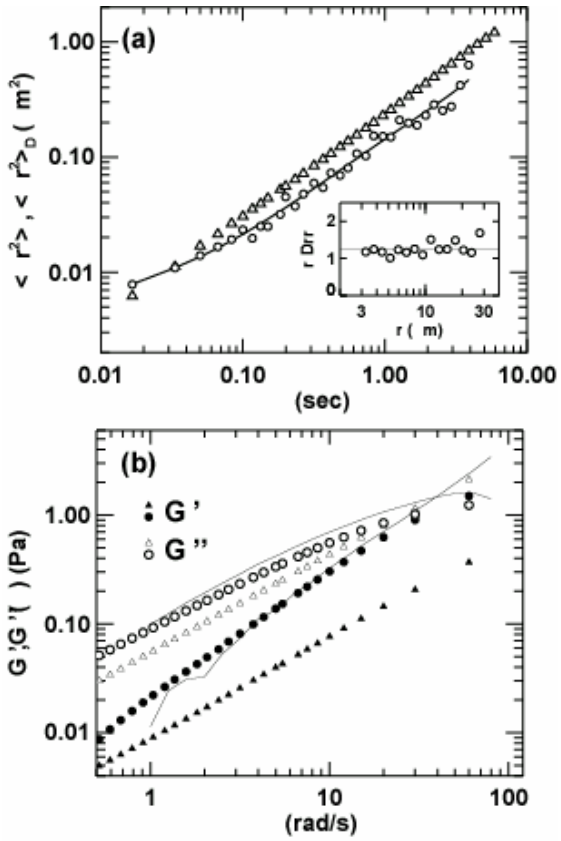

Fig. 1.6. The comparison of one- and two-particle microrheology to bulk measurements in a guar solution seen by Crocker et al. (Crocker, et al. 2000) (a) Comparison of the one-particle MSD (triangles) and distinct MSD (circles) of 0.20 μm diameter beads in 0.25% weight guar solution. Due to the heterogeneous nature of the medium, the curves differ by a factor of two. The solid line is a smooth fit to the data used for calculating rheology. (b) The elastic (filled circles) and loss (open circles) moduli calculated using the distinct MSD showing a crossover at high frequencies are in good agreement with the mechanical bulk measurement (solid curves). The moduli calculated using the one-particle MSD (triangles) do not agree. (reprinted with permission from Crocker, et al. 2000)

1.6 Summary

Microrheological techniques are powerful methods to characterize the mechanics and structure of novel and complex materials on length scales much shorter than those measured with bulk techniques. In an incompressible, homogeneous material the response of an individual probe due to external forcing or thermal fluctuations is a reflection of the bulk, viscoelastic properties of the surrounding medium. In heterogeneous materials, the motion of individual beads allows characterization of local mechanics while macroscopic rheological response is obtained by calculating the cross-correlated motion of the tracers from the same data. By combining the local and macroscopic measurements, a new understanding of how structure and mechanical response at the micron length scale relates to the bulk material properties emerges. Only microliter sample volumes are required, allowing the application of rheological techniques to materials too costly or difficult to synthesize in large quantities, or systems that are inherently small like living cells. Furthermore, viscoelastic response can be measured at frequencies ranging from 0.01 Hz to 10^5 Hz, much larger than the range of traditional mechanical measurements, allowing direct measurements of high frequency response in a wide range of soft materials. These techniques allow the study of both new systems and different material properties than conventional methods, and open new possibilities for understanding the microscopic properties of complex materials.

The authors would like to thank the following people for useful discussions: F. Amblard, A. Bailey, A.R. Bausch, L. Cipelletti, J.C. Crocker, B.R. Dasgupta, B. Frisken, P.D. Kaplan, A. Levine, F. MacKintosh, T. Mason, H.D. Ou-Yang, V. Trappe, C. Schmidt, E. Weeks.

Appendix: Descriptions of Experimental Apparati

Here we discuss in detail the various experimental techniques used in our lab: Dynamic Light Scattering, Diffusing Wave Spectroscopy, and Video-based particle tracking methods. For each technique, we use embedded colloidal particles that are purchased commercially from Bangs Laboratories Inc. (Fishers, IN), Molecular Probes (Eugene, OR), or IDC, Interfacial Dynamics Corporation (Portland, OR). A variety of surface chemistries that include surface-bound carboxyl, amine, or sulfate groups, sizes that range from approximately 20 nm to several microns, and different fluorescent dyes are available.

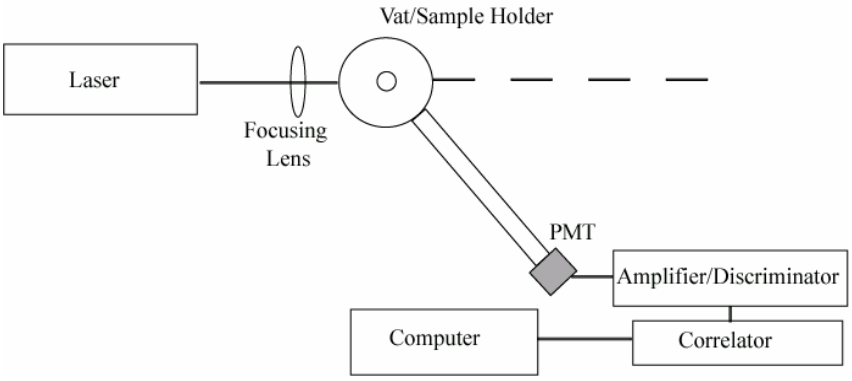

Fig. A.1. A standard dynamic light scattering setup

A.1 Dynamic Light Scattering

The typical dynamic light scattering apparatus includes a light source, a goniometer that contains the sample and defines the scattering geometry, a detector, and a digital correlator that calculates the intensity autocorrelation function in real time, as shown in Fig. A.1 (Berne and Pecora 2000; Pecora 1985; Johnson and Gabriel 1981). The common light source is a continuous wave laser, a coherent, monochromatic source of light with an emission wavelength in the range of 400-700 nm. For single light scattering measurements, our lab employs a Coherent Innova 300-series Argon-Ion Laser (Santa Clara, CA), which is operated at a wavelength of 514.5 nm; the laser power at the sample is typically in

the range of 50-300 mW. The operational wavelength is not critical, although the absorbance lines for a sample are avoided to prevent local heating, convection, and thermal lensing effects. The excitation wavelengths for fluorescent samples are also rejected. In cases where the excitation spectrum is wide, and it is not possible to eliminate fluorescence, filters are used to prevent any small emitted signal from reaching the detector. Plane-polarized light is required, as fluctuations in polarization give rise to undesired fluctuations in the intensity of the scattered light. To reduce mechanical vibrations, the experiment is often placed on an air-cushioned optical table, and to prevent relative movement of the laser and the sample, all optical elements are placed on the same plate.

The goniometer holds the sample and defines the scattering geometry. Several commercial goniometers are available; our lab uses models manufactured by Brookhaven Instruments (Holtzville, NY) and ALV (Langen, Germany). An entrance lens is used to focus the laser to a beam diameter of 50-100 microns, which increases the intensity of each coherence area, or speckle. Sample cells made from optical quality glass are used to reduce scattering and unwanted reflections from irregularities on the surface. Cylindrical vials are used for measurements at multiple scattering angles and are positioned such that the laser beam passes through the center of the vial; square cells are also useful for measurements at a fixed scattering angle of 90 degrees. Often the vial is placed in a vat filled with a fluid such as decalin or toluene with an index of refraction nearly equal to that of glass, in order to reduce the refraction and scattering at the vial surface. A window along the circumference of the vat allows the scattered light to reach the detector, which is placed on an arm that rotates about the center of the vial and collects the light at various angles. Typically, scattering angles ranging from 15 to 150 degrees are accessible, corresponding to q-vectors in the range of approximately 4-30 μm^{-1} (using Eqn. 1.46). At smaller angles, flare or scattering from large dust particles can dominate the signal and prevent good measurements of the particle mean-squared displacements (MSD). Using multiply filtered solutions may reduce the amount of dust present in the sample.

Detection optics, which include a series of lenses and pinholes or a fiber optic cable, define the scattering volume and collect the scattered light. A bright speckle occurs when light interferes constructively at the detector and the angular extent of a each speckle is given by: $\Delta\theta = \lambda/l$, where λ is the wavelength of the incoming light and l is the size of the beam in the scattering volume. For a beam of 50 microns in diameter that passes through a vial of 5 mm in diameter, the speckle size will be roughly 25 microns in width and 2.5 mm in height at a distance of 0.5 m from the center of the beam. The detector is typically positioned at a specific distance from the scattering volume to ensure that the collection area is limited to 1-2 speckles. When larger numbers of speckles are collected with traditional pinhole optics systems, their fluctuations tend to cancel and reduce the overall signal; however, this effect is not observed in fiber coupled systems (Gisler et. al., 1995). The detector typically consists of a pho-

tomultiplier tube (PMT), which is mounted on the goniometer arm and collects the incoming photons at a specific angle. Within the PMT, each photon strikes the cathode and emits an electron that is accelerated and collides with a dynode, which in turn emits several electrons. The current passes through a series of additional dynodes, amplifying a single electron roughly 10^6 times (Pecora 1985). Once one photon strikes the cathode of the PMT, there is a time delay before another photon may be detected. This "dead time" is due to the electron transit time and is typically in the range of tens of nanoseconds, setting a lower limit on the temporal resolution of this device. For most DLS measurements, this transit time is much shorter than any time scale of interest.

The amplified signal from the PMT is passed to a pulse amplifier discriminator circuit (PAD) that converts the small incoming voltage pulses into standard logic pulses of defined duration and height, which are then passed to the correlator. Typically PADs that are designed specifically for spectroscopy applications are used. The amplifier discriminator sets a threshold level for the incoming pulses in order to reject the low voltage signals that arise from spurious electrons, which are inadvertently amplified through the cascade circuit. In addition to these rogue electrons, positive ions are occasionally generated at some point in the electron cascade and return to the cathode or an early dynode to initiate a second cascade. In this case, a second pulse follows the first by several hundred nanoseconds and results in a peak in the correlation function at short delay times. The shortest delay times used experimentally are usually in the microsecond range, and this "afterpulsing" peak is not observed.

In cases where the short time dynamics are of interest, the scattered light is directed by a beam splitter onto two independent PMTs, which are processed by two amplifier discriminator circuits and the output of both is passed to the correlator. A pseudo-cross-correlated signal is then obtained, $\langle I_A(t) I_B(t+\tau) \rangle$ where the indices A and B distinguish the signals received by the two PMTs. The cross-correlation also reduces dead time effects (Weitz and Pine 1993).

After processing by the amplifier-discriminator, the signal is then transmitted to a digital correlator that calculates the intensity autocorrelation function in real time. The correlator is typically available as a PCI or ISA compatible card with a software interface. A range of delay times is available, and the shortest time is approximately 10 - 25 nanoseconds. Through the software interface, the number of channels, or delay times that are calculated, is selected and the spacing of the channels is also specified. Often the last few channels are shifted out to very long times to allow an independent measure of the baseline intensity, which is used to normalize the correlation function.

In order to calculate the mean squared displacement of the particles reliably, the intensity auto correlation function must be calculated with good statistical accuracy. There are two issues that reduce the signal to noise ratio: the finite intensity of the incoming light, and the limited duration of the experiment. The output signal from the PAD is typically in the range of one hundred thousand of photons per second, expressed as a count rate of 100 kHz. The photon counting

statistics are Poisson whereby the errors are given roughly by $N^{1/2}$, where N is the number of independent measurements. For a count rate of 100 kHz, the counting error would be roughly 0.3%; however, for a count rate of only 100 Hz, the counting error would be much larger, of order 10%. Additionally, for such low count rates the amount of noise present in the data becomes significant. The noise level is primarily due to the "dark current" of the PMT and is roughly 50 Hz, although the level varies depending on the details of the detector. This dark current arises from thermally excited electrons that produce an anode current even in the absence of any incoming light. In rare cases where the signal is so small that the dark current noise is appreciable, the PMT may be cooled to reduce the contribution of these thermal electrons. Alternatively, when the scattering signal is very large, some attenuation may be required; in general, count rates of greater than 1 MHz cause a nonlinear response, and count rates greater than 20 MHz damage the photosensitive PMT.

The second consideration in the statistical accuracy of the correlation function is the duration of the experiment. For simple fluids, the field correlation function, given in Eqn. 1.45 can be re-written as:

$$g_1(\tau) = \exp\left[-q^2 D\tau\right] \tag{1.51}$$

by substituting $<\Delta r^2(\tau)>=6D\tau$. The decay time is thus given by $1/q^2D$. Although viscoelastic materials will display a different dependence on τ, an estimate of the decay time can similarly obtained. The square root of the ratio of the decay time to the duration of the experiment gives a rough estimate of the statistical uncertainty in the MSD. For errors to be of order 3%, the duration must be is at least one thousand times longer than any decay time, a criterion that is easy to meet at large angles but more challenging at smaller angles due to the q^{-2} dependence on wave-vector. We collect data for roughly an hour at each angle to ensure sufficient statistical accuracy. Long experiments are not possible in time-evolving systems that may sediment or undergo chemical reactions during the course of the measurement. In this case, many consecutive short runs may be averaged together to obtain the MSD. Another disadvantage of long collection times is the increased likelihood of measuring contributions from stray dust particles or other contaminants that are present in solution; careful sample preparation will reduce this possibility.

For DLS measurements, only samples that are nearly transparent may be used in order to insure that each incoming photon is scattered only once before reaching the detector. For fluids or low contrast polymer solutions, a small amount of colloidal particles are added to a final volume fraction of $10^{-5} - 10^{-6}$. Typically, the scattering signal from the colloidal particles is significantly larger than the scattering from the solvent. For cloudy and opaque samples, single light scatter-

ing measurements are not possible, and the Diffusing Wave Spectroscopy (DWS) method should be used.

A.2 Diffusing Wave Spectroscopy

The Diffusing Wave Spectroscopy (DWS) apparatus is similar to that of the single light scattering experiment, and consists of a laser source, a simple optical train and sample holder, a detector, and digital correlator (Pine, et. al., 1988). The optical train allows for two boundary conditions, in which either a collimated or focused beam impinges on the sample cell. There are two experimental geometries: forward and backscattering. Our lab typically employs the forward scattering geometry, as shown in Fig. A.2. Higher laser powers are required for DWS measurements than for single scattering experiments and the laser power at the sample is roughly 100mW. Additionally, the coherence length of the laser is critical in DWS and must be larger than the longest paths of the scattered light through the sample, to insure that these paths are not discarded. The coherence length is increased by the addition of an intercavity etalon in our Coherent Innova 300 series Argon-ion laser (Santa Clara, CA) that insures operation in a single longitudinal mode. Photons that are multiply scattered report an angular average and lose their q-dependence; thus, a goniometer is not required. Multiply scattered light is depolarized and signals of equal intensity are found with polarization parallel or perpendicular to the incident beam. However, because each polarization is independent, this reduces the signal to noise ratio and causes the intercept of the intensity correlation function to fall to 0.5. To prevent this, a polarization analyzer is placed before the detector to restrict the scattered light to a single polarization.

Often in DWS experiments, the timescales of interest are extremely short and are comparable to the dead time of the PMT. In order to measure the dynamics

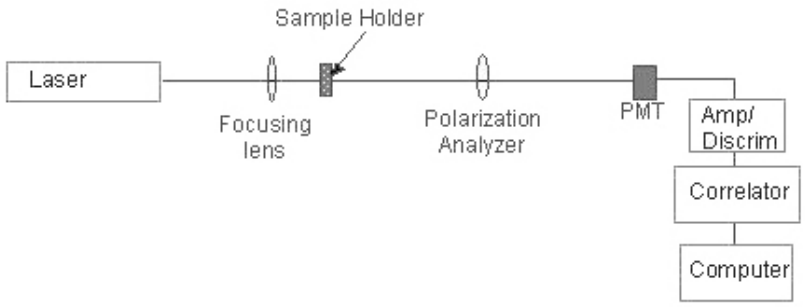

Fig. A.2. Diffusing Wave Spectroscopy setup.

of the sample on these timescales, a pseudo-cross-correlated signal is used. Cross-correlation also reduces afterpulsing effects, which occur at timelags of roughly 100 nanoseconds. For DWS experiments, the volume fraction of the embedded colloidal spheres is large, roughly 10^{-2}, in order to insure that the transport mean path, l^* is a small fraction of the length of the sample chamber, l. The ratio of l/l^* is typically greater than five. The mean free path is determined by comparing the transmitted intensity of a reference sample, whose transport mean path is known, to the experimental sample (Dasgupta, et. al. 2001).

A.3 Video Microscopy

Several of the microrheological techniques rely on accurately tracking the time evolved positions of individual probe particles. Laser Deflection Particle Tracking (Mason, et al. 1997, Schnurr, et al. 1997) measures the motion of individual beads with subnanometer precision at frequencies up to 50 kHz. This technique has excellent spatiotemporal resolution but is not designed to observe the dynamics of large ensembles of beads easily. Our lab uses video microscopy to follow the dynamics of ~100 beads simultaneously with a spatial resolution of 10 nm and temporal resolution of ~30 Hz. The time and spatial resolution of a particle tracking experiment with video microscopy relies on both the hardware used to capture images and the software algorithms used to detect particle centers. In the simplest setup an analog CCD camera (COHU, San Diego, CA) is attached to the side port of an optical microscope (Leica, Bannockburn, IL) and 480 x 640 pixel images are captured with a S-VHS video cassette recorder at a rate of 30 images per second. For most experiments, an eight bit analog, uncooled monochrome CCD camera with a variable shutter speed is sufficient. Monochrome CCD cameras are preferable to color cameras because they are more sensitive to subtle brightness variations, and are significantly cheaper. A larger dynamic range may be necessary for experiments with very dim or low contrast particles. The videotape of particle dynamics is then digitized by a computer equipped with a frame grabber card; digital images are analyzed to determine the particle positions in each frame.

For one micron spheres, images are typically obtained with bright field microscopy using a 40x air objective at a magnification of 250 nm/CCD pixel. In order for particle tracking algorithms to accurately determine particle centers, the number of pixels subtended by the image of each particle must be four or more CCD pixels. The image magnifications necessary to achieve this diameter will change based on the size of the embedded probe and if particles are imaged with bright field or fluorescence microscopy.

Colloidal particles are commercially available in sizes between 20 nm and several microns in diameter. The diffraction limited resolution, d, of a microscope is $d = 0.61 * \lambda / N.A.$ where $N.A.$ is the numerical aperture of the objective

used and λ is the wavelength of light. For light microscopy, this resolution limit is a few hundred nanometers. Colloidal spheres larger than this resolution limit can be observed directly with bright field microscopy. For smaller sizes, it is possible to use fluorescence microscopy to image dyed colloids. In either method, the colloidal particle position is observed as a circularly symmetric Gaussian image intensity profile centered at its geometrical center. In general, particle tracking routines are able to locate particle positions with subpixel accuracy by iterating an initial position, which is determined as the brightest pixel in a local region, with the offsets in position, determined by calculating the brightness-weighted centroid of the surrounding region, to refine the location of the peak in brightness within a single pixel. At a magnification of 100x (10 pixels/micron), subpixel accuracy corresponds to a spatial resolution of 10 nm, an order of magnitude better than diffraction limited resolution! Because these particle tracking routines depend on variations of brightness over distances larger than the diffraction limited resolution, the numerical aperture of the objective does not affect the accuracy of detecting centers. However, a lower numerical aperture increases the depth of focus and projection error of particle motion perpendicular to the field of view increases.

The shutter speed of the CCD camera sets the exposure time, τ_e, of a single image. If the exposure time is long enough to allow significant particle motion, the microscope image of the particle will not be circularly symmetric which results in a decreased ability of finding an accurate center. The shutter speed is set so a probe of radius a embedded in a fluid of viscosity η diffuses less than the spatial resolution, 10 nm, in τ_e. We calculate the one dimensional root mean-squared displacement, $< \Delta x^2(\tau_e) >^{1/2} = \left(2D\tau_e\right)^{1/2} \leq 10$ nm, where the diffusion constant, D, is determined by the Einstein relation, $D = k_B T / 6\pi\eta a$. For a typical experiment with a one micron probe embedded in a medium with a viscosity of 0.001 Pa*sec, a shutter speed of 1 msec is sufficient.

Typically, a single CCD image is captured with alternate rows of pixels captured every 1/60 of a second. This allows the temporal resolution of video microscopy to be extended to 60 Hz by extracting the even and odd rows of the image to give two 240 x 640 images captured every 1/60 of a second (Crocker and Grier 1996). Without extracting the separate fields, the full 480 x 640 image is a superposition of two vertically interlaced half frame images, or fields, taken 1/60 second apart. If the particle moves significantly during that time, it is impossible to resolve an accurate particle center. A 100 nm particle in water (η=0.001 Pa*sec) imaged at a magnification of 10 pixels/μm (100x oil immersion objective) moves 100 nm, or one pixel, in 1/60 sec. Without a field analysis, the particle tracking resolution decreases by an order of magnitude and the particle dynamics at the shortest lag times near 1/30 sec, are seriously affected. Unless the particle motion between captured fields is beneath the noise floor of the particle tracking routines, the short time dynamics analyzed with an inter-

laced image will be affected by image averaging error. The resolution with a field analysis is significantly improved for the horizontal direction, but in the vertical direction the resolution is often adversely affected because of the number of pixels subtended by the image in that direction is halved.

The CCD camera BNC output is directly connected to a television for viewing and a high quality S-VHS cassette recorder (Sanyo, Chatsworth, CA) to record time series of images at video rate. A computer equipped with a frame grabber card is interfaced with the video cassette recorder to digitize images at rates accessible to the available RAM of the computer by capturing images for a short time and then pausing the movie while images are written to a file. In most cases, the limitation to writing images directly to the hard drive at video rates is that it takes longer than 1/30 second to write an image from RAM to the disk. With a special configuration of the hardware of a personal computer and custom software, it is now possible to write full frame images directly to the hard drive at video rates in standard movie file format (Keller, Schilling et al. 2001). Commercially available software (Universal Imaging Corporation, Downingtown, PA; Scion, Frederick, MA) to control frame grabbing hardware is also available.

Digital cameras (Hamamatsu, Bridgewater, NJ) now offer an alternative to traditional CCD cameras and allow control over pixel resolution, integration time, size and capture rate of the images. This enables us to optimize image quality for very dim particles or achieve capture rates faster than a traditional CCD camera by decreasing resolution and frame size. Digital movies are converted to a three-dimensional tiff stack of images and software is used to locate colloidal features in each image. We use particle tracking routines developed by John Crocker and David Grier (Crocker and Grier 1996). An online tutorial of this method with software routines written in IDL is maintained by John Crocker and Eric Weeks and is available at http://glinda.lrsm.upenn.edu/~weeks/idl/. The particle tracking algorithms are comprised of three steps: identification of appropriate parameters to detect the position of desired particles appearing in a single image, using a macro to automate the identification for every tiff image in a 3D tiff array and linking the positions found in each frame to form particle trajectories. The particle identification software detects bright ‘spots’ against a dark, zero intensity background pixel map. A ‘spot’, or feature, is a region of locally higher intensity with a circularly symmetric Gaussian brightness profile across its diameter. Because our tracking programs are dependent on variations in brightness; the image contrast should be maximized without saturating the image so there is a unique maximum in the brightness profile across the bead image.

To identify features, the tiff image is smoothed using a spatial bandpass filter with the lower bound of allowed wavelengths set to retain subtle variations in brightness (usually one pixel) and the upper bound set to the average diameter of the features. After smoothing the image, the average background intensity is subtracted so the final image is a low intensity background with sharply peaked

circular 'spots' where the original particle images are. After locating the brightest pixels in a given region, a circular Gaussian mask with a diameter greater than or equal to the upper bound of the spatial bandpass is iterated around this guess to refine the located center of these circular peaks in the image brightness. Given a smoothed image and diameter of a Gaussian mask, our feature finding program will return a five dimensional array with the x-centriod, y-centroid, integrated brightness, radius of gyration and eccentricity for each feature found. To obtain subpixel accuracy, we choose the diameter of the mask to be slightly larger than that subtended by the particle image. This ensures the algorithm is able to find the unique maximum of the feature upon iteration.

This feature finding routine is very sensitive and will detect many possible particles. To separate the actual particles from false identifications, we further discriminate the found features based on their integrated brightness, eccentricity and radius of gyration. Colloidal features will fall into a broad cluster around certain values of radius of gyration and brightness. For any given image, false particle identifications will tend to lie outside this target cluster and can be clipped. Eccentricity, a geometrical measure of how circular an ellipse is, ranges from zero for circles and one for lines. Since we track circular features, we can set an upper bound on the eccentricity of 0.2 to allow for slight deviations from circular symmetry. We find the parameters that successfully eliminate rogue particle identifications for a single image and use identical bounds for subsequent images. It is often useful to overlay the located particle positions with the original microscope image to visually check particle identifications.

Once colloidal particles are located in a sequence of video images, particle positions in each image are correlated with positions in later images to produce trajectories. To track more than one particle, care is required to uniquely identify each particle in each frame (Crocker and Grier 1996). In practice, the typical distance a particle moves between images must be significantly smaller than the typical interparticle spacing. Otherwise, particle positions will be confused between snapshots. Particles that are a few hundred nanometers in diameter typically diffuse a distance smaller than their diameters between frames and, therefore, relatively high concentrations of particles can be used.

Because particles can move in and out of the focused field of view, it is useful to include a memory function in the tracking algorithm that allows gaps in a trajectory where a feature is not found. The last known locations of missing particles are retained in case unassigned particles reappear sufficiently nearby to resume the trajectory. Using a memory function allows the length of individual tracks to be maximized, therefore greatly increasing the statistics for the mean-squared displacement (MSD). Trajectories are identified for every feature in the field of view and saved as an array. In a typical multiparticle tracking experiment, millions of positions are assigned to thousands of particle trajectories. We usually require 1000 independent events to calculate the MSD at a given lag time. The number of events, or independent particle displacements, increases with both the number of particles in a field of view and the length of particle

tracks (Valentine, et. al. 2001). For an experiment tracking forty beads with a diameter of one micron in a viscous medium of 0.001 Pa*sec, around ten minutes of video is required to calculate the MSD to lag times of one minute.

A.4 Obtaining $G^*(\omega)$ from $\left\langle \Delta\vec{r}^2(t) \right\rangle$

In all the methods discussed, we desire to obtain knowledge of the complex shear modulus from the bead dynamics. In order to relate the mean-squared displacement of embedded Brownian probes, $\left\langle \Delta\vec{r}^2(t) \right\rangle$, to a frequency dependent complex modulus, $G^*(\omega)$, using the generalized Stokes-Einstein relation, it is necessary to calculate the numerical Laplace transform of $\left\langle \Delta\vec{r}^2(t) \right\rangle$ to obtain $\tilde{G}(s)$ using Eqn. 1.37. We then fit $\tilde{G}(s)$ to a continuous functional form in the real variable s and substitute $s=i\omega$ into $\tilde{G}(s)$ to obtain $G^*(\omega) = G'(\omega) + iG''(\omega)$. While direct, this method of transforming the mean-squared displacement can introduce significant errors in the moduli obtained. The numerical Laplace transform is typically implemented by selecting a frequency s, multiplying $\left\langle \Delta\vec{r}^2(t) \right\rangle$ by a decaying exponential and integrating using the trapezoid rule. While this method is very accurate within frequency extremes, it introduces errors near frequency extremes due to truncation of the data set. These errors are usually significant for data within a decade of either extrema. Additionally, the analytic continuation of $\tilde{G}(s)$ requires finding an appropriate functional form of discrete data. Without an accurate functional form of the discrete data, significant errors can result in the elastic and loss complex moduli.

To overcome these errors, Mason, et. al. (Mason 2001) developed a method to estimate the transforms algebraically by using a local power law around a frequency of interest, ω, and retaining the leading term:

$$\left\langle \Delta\vec{r}^2(t) \right\rangle \approx \left\langle \Delta\vec{r}^2(1/\omega) \right\rangle (\omega t)^{\alpha(\omega)} \tag{1.52}$$

where $\left\langle \Delta\vec{r}^2(1/\omega) \right\rangle$ is the magnitude of at $t=1/\omega$ and

$$\alpha(\omega) \equiv \left. \frac{d \ln \left\langle \Delta\vec{r}^2(t) \right\rangle}{d \ln t} \right|_{t=1/\omega} \tag{1.53}$$

is the power law exponent describing the logarithmic slope of $\left\langle \Delta \vec{r}^2(t) \right\rangle$ at t=1/ω. The Fourier transform, $\Im\left\langle \Delta \vec{r}^2(t) \right\rangle$, of the power law is directly evaluated:

$$i\omega \Im\left\langle \Delta r^2(t) \right\rangle \approx \left\langle \Delta r^2(1/\omega) \right\rangle \Gamma\left[1+\alpha(\omega)\right] i^{-\alpha(\omega)} \tag{1.54}$$

where Γ is the gamma function. Using a local power law approximation implicitly assumes that contributions to the transform integral from the behavior of $<\Delta r^2(t)>$ at times different than $1/\omega$ can be neglected. By substitution into the Fourier representation of the GSER and the use of Euler's equation, we obtain:

$$\begin{aligned} G'(\omega) &= \left|G^*(\omega)\right| \cos(\pi\alpha(\omega)/2) \\ G''(\omega) &= \left|G^*(\omega)\right| \sin(\pi\alpha(\omega)/2) \end{aligned} \tag{1.55}$$

where

$$\left|G^*(\omega)\right| \approx \frac{k_B T}{\pi a \left\langle \Delta r^2(1/\omega) \right\rangle \Gamma\left[1+\alpha(\omega)\right]} \tag{1.56}$$

These relations provide a direct physical intuition of how the elastic and loss moduli depend on $<\Delta r^2(t)>$. In a pure viscous medium, the sphere diffuses and $\alpha \approx 1$ resulting in a dominant loss modulus. Constrained in a pure elastic medium, the α approaches zero and the elastic modulus dominates.

While this estimation method is convenient and intuitive to use, it can fail to give an accurate estimation of the moduli when the mean-squared displacement is sharply curved with a rapidly changing slope. These regions can be of particular interest because such changes reflect significant relaxation times of the sample. To account for these issues, modifications (Dasgupta et. al. 2002) have been made to Eqn. 1.56 to better account for curvature in the mean-squared displacement and give improved estimates of the moduli in these regions.

A-Hassan E, Heinz WF, Antonik MD, D'Costa NP, Nageswaran S (1998) Relative microelastic mapping of living cells by atomic force microscopy. Biophysical Journal 74:1564-1578

Amblard F, Maggs AC, Yurke B, Pargellis AN, Leibler S (1996) Subdiffusion and anomalous local viscoelasticity in actin networks. Physical Review Letters 77:4470-4473

Amblard F, Yurke B, Pargellis A, Leibler S (1996) A magnetic manipulator for studying local rheology and micromechanical properties of biological systems. Review of Scientific Instruments 67:818-827

Ashkin A (1992) Forces of a single-beam gradient laser trap on a dielectric sphere in the ray optics regime. Biophysical Journal 61:569-582

Ashkin A (1997) Optical trapping and manipulation of neutral particles using lasers. Proceedings of the National Academy of Sciences of the United States of America 94:4853-4860

Ashkin A (1998) Forces of a single-beam gradient laser trap on a dielectric sphere in the ray optics regime. Methods in Cell Biology 55:1-27

Bausch AR, Hellerer U, Essler M, Aepfelbacher M, Sackmann E (2001) Rapid stiffening of integrin receptor-actin linkages in endothelial cells stimulated with thrombin: A magnetic bead microrheometry study. Biophysical Journal 80:2649-2657

Bausch AR, Möller W, Sackmann E (1999) Measurement of local viscoelasticity and forces in living cells by magnetic tweezers. Biophysical Journal 76:573-579

Bausch AR, Ziemann F, Boulbitch AA, Jacobson K, Sackmann E (1998) Local measurements of viscoelastic parameters of adherent cell surfaces by magnetic bead microrheometry. Biophysical Journal 75:2038-2049

Berne BJ, Pecora R (2000) Dynamic Light Scattering with applications to chemistry, biology, and physics. Dover, Mineola

Binning G, Quate CF, Gerber C (1986) Atomic Force Microscope. Physical Review Letters 56:930-933

Block SM (1992) Making light work with optical tweezers. Nature 360:493-495

Bottomley LA, Coury JE, First PN (1996) Scanning probe microscopy. Biophysical Journal 74:1564-1578

Butt H-J, Jaschke M (1995) Thermal noise in atomic force microscopy. Nanotechnology 6:1-7

Crick F, Hughes A (1950) The physical properties of the cytoplasm. Experimental Cell Research 1:37-80

Crocker JC, Grier DG (1996) Methods of digital video microscopy. Journal of Colloid and Interface Science 179:298-310

Crocker JC, Valentine MT, Weeks ER, Gisler T, Kaplan PD, Yodh AG, Weitz DA (2000) Two-point microrheology of inhomogeneous soft materials. Physical Review Letters 85:888-891

Dasgupta BR, Tee S-Y, Crocker JC, Frisken BJ, Weitz DA (2001) Microrheology of polyethylene oxide using diffusing wave spectroscopy and single scattering. Physical Review E 65:051505

Dinsmore AD, Weeks ER, Prasad V, Levitt AC, Weitz DA (2001) Three-dimensional confocal microscopy of colloids. Applied Optics 40:4152-4159

Domke J, Radmacher M (1998) Measuring the elastic properties of thin polymer films with the AFM. Langmuir 14:3320-3325

Drake B, Prater CB, Weisenhorn AL, Gould SAC, Albrecht TR, Quate CF, Channell DS, Hansma HG, Hansma PK (1989) Imaging crystals, polymers, and biological processes in water with AFM. Science 243:1586-1589

Dvorak JA, Nagao E (1998) Kinetic analysis of the mitotic cycle of living vertebrate cells by atomic force microscopy. Experimental Cell Research 242:69-74

Fabry B, Maksym GN, Butler JP, Glogauer M, Navajas D, Fredberg JJ (2001) Scaling the microrheology of living cells. Physical Review Letters 87:148102(4)

Fällman E, Axner O (1997) Design for fully steerable dual-trap optical tweezers. Applied Optics 36:2107-2113

Feneberg W, Westphal M, Sackmann E (2001) Dictyostelium cells' cytoplasm as an active viscoplastic body. European Biophysical Journal 30:284-294

Ferry J (1980) Viscoelastic properties of polymers. Wiley, New York

Ford NC (1985) Light Scattering Apparatus. In: Pecora R (ed) Dynamic light scattering: Applications of photon correlation spectroscopy. Plenum, London pp. 7-58

Freundlich H, Seifriz W (1922) Ueber die elastizität von solen und gelen. Zeitschrift fur physikalische chemie 104:233

Gisler T, Weitz DA (1998) Tracer microrheology in complex fluids. Current Opinion in Colloid and Interface Science 3:586-592

Gisler T, Weitz DA (1999) Scaling of the microrheology of semidilute F-actin solutions. Physical Review Letters 82:1606-1609

Gisler T, Ruger H, Egelhaaf SU, Tschumi J, Schurtenberger P, Ricka J (1995) Mode-selective dynamic light scattering: theory versus experimental realization. Applied Optics 34:3546-3553

Gittes F, Schnurr B, Olmsted PD, MacKintosh FC, Schmidt CF (1997) Microscopic viscoelasticity: shear moduli of soft materials determined from thermal fluctuations. Physical Review Letters 79:3286-3289

Gittings MR, Cipelletti L, Trappe V, Weitz DA, In M, Marques C (2000) Structure of guar in solutions of H_20 and D_20: An ultra-small-angle light scattering study. Journal of Physical Chemistry B 104:4381-4386

Goldman WH, Ezzell RM (1996) Viscoelasticity in wild-type and vinculin-deficient mouse F9 embryonic carcinoma cells examined by atomic force microscopy. Experimental Cell Research 226:234-237

Heilbronn A (1922) Eine neue methode zur bestimmung der viskosität lebender protoplasten. Jahrbuch der Wissenschaftlichen Botanik 61:284-338

Henderson E, Haydon PG, Sakaguchi DS (1992) Actin filament dynamics in living glial cells imaged by atomic force microcopy. Science 257:1944-1946

Hénon S, Lenormand G, Richert A, Gallet F (1999) A new determination of the shear modulus of the human erythrocyte membrane using optical tweezers. Biophysical Journal 76:1145-1151

Hertz H (1881) Über die berührung fester elastischer körper. J. Reine Agnew. Mathematik 92:156-171

Hiramoto Y (1969) Mechanical properties of the protoplasm of the sea urchin egg. Experimental Cell Research 56:201-218

Hoh JH, Schoenenberger CA (1994) Surface morphology and mechanical properties of MDCK monolayers by atomic force microscopy. Journal of Cell Science 107:1105-1114

Hough LA, Ou-Yang HD (1999) A new probe for mechanical testing of nanostructures in soft materials. Journal of Nanoparticle Research 1:495-499

Johnson CS, Gabriel DA (1995) Laser Light Scattering. Dover, New York.

Joosten JGH, Gelade ETF, Pusey PN (1990) Dynamic light scattering by non-ergodic media: Brownian particles trapped in polyacrylamide gels Physical Review A 42:2161-2175

Kao HP, Verkman AS (1994) Tracking of single fluorescent particles in three dimensions: the use of cylindrical optics to encode particle position. Biophysical Journal 67:1291-1300

Kasas S, Thomson NH, Smith BL, Hansma PK, Mikossy J, Hansma HG (1997) Biological applications of the AFM: from single molecules to organs. International Journal of Imaging Systems and Technology 8:151-161

Keller M, Schilling J, Sackmann E (2001) Oscillatory magnetic bead rheometer for complex fluid microrheometry. Review of Scientific Instruments 72:3626-3624

King M, Macklem PT (1977) Rheological properties of microliter quantities of normal mucus. Journal of Applied Physiology 42:797-802

Landau LD, Lifshitz EM (1986) Theory of Elasticity. Pergamon Press, Oxford

Larson RG (1999) The structure and rheology of complex fluids. Oxford University Press, New York

Levine AJ, Lubensky TC (2000) One- and two-particle microrhelogy. Physical Review Letters 85:1774-1777

Macosko CW (1994) Rheology: principles, measurements, and applications. VCH, New York

Mahaffy RE, Shih CK, MacKintosh FC, Käs J (2000) Scanning probe-based frequency-dependent microrheology of polymer gels and biological cells. Physical Review Letters 85:880-883

Mason TG (2000) Estimating the viscoelastic moduli of complex fluids using the generalized Stokes-Einstein equation. Rheologica Acta 39: 371-378

Mason TG, Ganesan K, Van Zanten JH, Wirtz D, Kuo SC (1997) Particle tracking microrheology of complex fluids. Physical Review Letters 79:3282-3285

Mason TG, Gang H, Weitz DA (1996) Rheology of complex fluids measured by dynamic light scattering. Journal of Molecular Structure 383:81-90

Mason TG, Gang H, Weitz DA (1997) Diffusing-wave spectroscopy measurements of viscoelasticity of complex fluids. Journal of the Optical Society of America 14:139-149

Mason TG, Gisler T, Kroy K, Frey E, Weitz DA (2000) Rheology of F-actin solutions determined from thermally driven tracer motion. Journal of Rheology 44:917-928

Mason TG, Weitz DA (1995) Optical measurements of the frequency-dependent linear viscoelastic moduli of complex fluids. Physical Review Letters 74:1250-1253

McGrath JL, Hartwig JH, Kuo SC (2000) The mechanics of F-actin microenvironments depend on the chemistry of probing surfaces. Biophysical Journal 79:3258-3266

Mio C, Gong T, Terray A, Marr DWM (2000) Design of a scanning laser optical trap for multiparticle manipulation. Review of Scientific Instruments 71:2196-2200

Mio C, Marr DWM (2000) Optical Trapping for the Manipulation of Colloidal Particles. Advanced Materials 12:917-920

Nemoto S, Togo H (1998) Axial force acting on a dielectric sphere in a focused laser beam. Applied Optics 37:6386-6394

Neto PAM, Nussenzveig HM (2000) Theory of optical tweezers. Europhysics Letters 50:702-708

Ou-Yang HD, (1999) Design and applications of oscillating optical tweezers for direct measurements of colloidal forces. In: Farinato RS and Dubin PL (eds) Colloid-Polymer Interactions: From Fundamentals to Practice. Wiley, New York, pp 385-405

Ovryn B (2000) Three-dimensional forward scattering particle image velocimetry applied to a microscopic field of view. Experiments in Fluids 29:S175-S184

Ovryn B, Izen SH (2000) Imaging of transparent spheres through a planar interface using a high numerical-aperture optical microscope. Journal of the Optical Society of America, A 17:1202-1213

Palmer A, Mason TG, Xu J, Kuo SC, Wirtz D (1999) Diffusing wave spectroscopy microrheology of actin filament networks. Biophysical Journal 76:1063-1071

Pine DJ, Weitz DA, Chaikin PM, Herbolzheimer E (1988) Diffusing Wave Spectroscopy. Physical Review Letters 60:1134-1137

Pusey PN, van Megen W (1989) Dynamic Light Scattering by non-ergodic media. Physica A 157:705-741

Putman CA, Werf KOVD, Grooth BGD, Hulst NFV, Greve J (1994) Viscoelasticity of living cells allows high resolution imaging by tapping mode atomic force microscopy. Biophysical Journal 67:1749-1753

Radmacher M, Cleveland JP, Fritz M, Hansma HG, Hansma PK (1994) Mapping interaction forces with the atomic force microscope. Biophysical Journal 66:2159-2165

Radmacher M, Fritz M, Hansma PK (1995) Imaging soft samples with the atomic force microscope: gelatin in water and propanol. Biophysical Journal 69:264-270

Radmacher M, Fritz M, Kasher CM, Cleveland JP, Hansma PK (1996) Measuring the viscoelastic properties of human platelets with the atomic force microscope. Biophysical Journal 70:556-567

Radmacher M, Tillmann RW, Fritz M, Gaub HE (1992) From molecules to cells - imaging soft samples with AFM. Science 257:1900-1905

Reif F (1965) Fundamentals of statistical and thermal physics. McGraw-Hill, Inc., New York

Rotsch C, Braet F, Wisse E, Radmacher M (1997) AFM imaging and elasticity measurements of living rat liver macrophages. Cell Biology International 21:685-696

Rotsch C, Radmacher M (2000) Drug-induced changes of cytoskeletal structure and mechanics in fibroblasts: an atomic force microscopy study. Biophysical Journal 78:520-535

Schmidt FG, Hinner B, Sackmann E, Tang JX (2000) Viscoelastic properties of semiflexible filamentous bacteriophage fd. Physical Review E 62:5509-5517

Schmidt FG, Ziemann F, Sackmann E (1996) Shear field mapping in actin networks by using magnetic tweezers. European Biophysics Journal 24:348-353

Schneider SW, Sritharan SW, Geibel JP, Oberleithner H, Jena B (1997) Surface dynamics in living acinar cells imaged by atomic force microscopy: identification of

plasma membrane structures involved in exocytosis. Proceedings of the National Academy of Sciences of the United States of America 94:316-321

Schnurr B, Gittes F, MacKintosh FC, Schmidt CF (1997) Determining microscopic viscoelasticity in flexible and semiflexible polymer networks from thermal fluctuations. Macromolecules 30:7781-7792

Shroff SG, Saner DR, Lal R (1995) Dynamic micromechanical properties of cultured rat atrial myocytes measured by atomic force microscopy. American Journal of Physiology 269:C286-C289

Sleep J, Wilson D, Simmons R, Gratzer W (1999) Elasticity of the red cell membrane and its relation to hemolytic disorders: an optical tweezers study. Biophysical Journal 77:3085-3095

Sneddon IN (1965) The relation between load and penetration in the axisymmetric Boussinesq problem for a punch of arbitrary profile. International Journal of Engineering Science 3:47-57

Tao NJ, Lindsay SM, Lees S (1992) Measuring the microelastic properties of biological material. Biophysical Journal 63:1165-1169

Tseng Y, Wirtz D (2001) Mechanics and multiple particle tracking microheterogeneity of α-actinin-crosslinked actin filament networks. Biophysical Journal 81:1643-1656

Valberg PA (1984) Magnetometry of ingested particles in pulmonary macrophages. Science 224:513-516

Valberg PA, Albertini DF (1985) Cytoplasmic motions, rheology, and structure probed by a novel magnetic particle method. Journal of Cell Biology 101:130-140

Valberg PA, Butler JP (1987) Magnetic particle motions within living cells: Physical theory and techniques. Biophysical Journal 52:537-550

Valberg PA, Feldman HA (1987) Magnetic particle motions within living cells: Measurement of cytoplasmic viscosity and motile activity. Biophysical Journal 52:551-561

Valentine MT, Dewalt LE, Ou-Yang HD (1996) Forces on a colloidal particle in a polymer solution: a study using optical tweezers. Journal of Physics: Condensed Matter (U.K.) 8:9477-9482

Valentine MT, Kaplan PD, Thota D, Crocker JC, Gisler T, Prud'homme RK, Beck M, Weitz DA (2001) Investigating the microenvironments of inhomogeneous soft materials with multiple particle tracking. Physical Review E 64:061506

van Megen W, Underwood SM, Pusey PN (1991) Nonergodicity parameters of colloidal glasses. Physical Review Letters 67:1586-1589

Velegol D, Lanni F (2001) Cell Traction Forces on Soft Biomaterials. I. Microrheology of Type I Collagen Gels. Biophysical Journal 81:1786-1792

Visscher K, Block SM (1998) Versatile optical traps with feedback control. Methods in Enzymology 298:460-479

Wang N, Butler JP, Ingber DE (1993) Mechanotransduction across the cell surface and through the cytoskeleton. Science 260:1124-1127

Wang N, Ingber DE (1994) Control of cytoskeletal mechanics by extracellular matrix, cell shape, and mechanical tension. Biophysical Journal 66:1281-1289

Wang N, Ingber DE (1995) Probing transmembrane mechanical coupling and cytomechanics using magnetic twisting cytometry. Biochemistry and Cell Biology 73:327-335

Weeks ER, Crocker JC, Levitt AC, Schofield A, Weitz DA (2000) Three-dimensional imaging of structural relaxation near the colloidal glass transition. Science 287:627-631

Weitz DA, Pine DJ, (1993) Diffusing-wave spectroscopy. In: Brown W (ed) Dynamic Light Scattering. Oxford University Press, Oxford, pp 652-721

Xue JZ, Pine DJ, Milner ST, Wu XL, Chaikin PM (1992) Non-ergodicity and light scattering from polymer gels. Physical Review A 46:6550-6563

Yagi K (1961) The mechanical and colloidal properties of Amoeba protoplasm and their relations to the mechanism of amoeboid movement. Comparative Biochemistry and Physiology 3:73-91

Yamada S, Wirtz D, Kuo SC (2000) Mechanics of living cells measured by laser tracking microrheology. Biophysical Journal 78:1736-1747

Zaner KS, Valberg PA (1989) Viscoelasticity of F-actin measured with magnetic particles. Journal of Cell Biology 109:2233-2243

Ziemann F, Rädler J, Sackmann E (1994) Local measurements of viscoelastic moduli of entangled actin networks using an oscillating magnetic bead micro-rheometer. Biophysical Journal 66:2210-2216